Newsletters on Stratigraphy, Vol. 54/1 (2021), 43–78 **Article**
Published online August 26, 2020; published in print January 2021

Integrated stratigraphy of the latest Barremian–early Albian interval in the western part of the Tethyan margin: new data from the Essaouira-Agadir Basin (Western Morocco)

Fabienne Giraud[1]*, Walid Hassanein Kassab[2], Emmanuel Robert[3], Etienne Jaillard[1], Jorge E. Spangenberg[4], Moussa Masrour[5], Mohamed S. Hammed[2], Mohamed F. Aly[2] and Khadija El Hariri[6]

With 13 figures, 4 plates and 1 table

Abstract. The Essaouira-Agadir Basin (EAB, Morocco) presents numerous and well-exposed outcrops of the Lower Cretaceous series. Here we present an integrated stratigraphic framework for the latest Barremian–early Albian, and for the western Tethys based on i) the identification of sedimentary discontinuities, ii) the establishment of a high-resolution ammonite and calcareous nannofossil biozonation, and iii) a carbon isotope record. Various sedimentary discontinuities corresponding to erosive surfaces were recognized within these deposits. Most of these surfaces are correlated within the EAB, and correspond to drops in sea level. The distribution of ammonite assemblages was calibrated with the standard Mediterranean zonation. Several ammonite index-species have been identified, in particular for the early Aptian and earliest late Aptian. This was crucial because the lower series are dominated by condensed sedimentation and temporal hiatuses. Most of the uppermost Barremian to lower Albian ammonite standard zones have been recognized. Four new and reliable calcareous nannofossil bioevents have been identified in the late Aptian allowing to revise the NC7 Zone. The taxonomic criteria used to define species markers of both NC8A and NC8B subzones have been specified, thereby improving the calibration of these subzones with ammonite biozones. The $\delta^{13}C_{carb}$ values from whole rock samples decrease from the late Aptian to the early Albian. The new biostratigraphic and chemostratigraphic scheme for the EAB allowed rather good correlations between sections from southern and northern Tethyan margins.

Key words. sedimentary discontinuities, ammonite and calcareous nannofossil biostratigraphy, carbon isotope stratigraphy, Aptian–Albian boundary, correlations

1. Introduction

In North Africa, the late Barremian–early Albian interval is marked by: (1) a widespread marine transgression (Hardenbol et al. 1998, Haq 2014), (2) tectonic events, materialized by syn-sedimentary deformation, local emergences, clastic deposits and rapid facies variations (e. g. Piqué et al. 1998, Guiraud et al.

Authors' addresses:
[1] Univ. Grenoble Alpes, IRD, Univ. Savoie Mont Blanc, CNRS, Univ. Gustave Eiffel, ISTerre, 38000 Grenoble, France
[2] Cairo University, Faculty of Science, Geology Department, Giza, Egypt
[3] Univ. Lyon, Université Claude Bernard Lyon 1, ENS de Lyon, CNRS, UMR 5276 LGL-TPE, F-69622 Villeurbanne, France
[4] Institute of Earth Surface Dynamics (IDYST), University of Lausanne, Géopolis, CH-1015 Lausanne, Switzerland
[5] Université Ibn Zohr, Faculté des Sciences, Département de Géologie, B. P. 8106, Cité Dakhla, Agadir, Morocco
[6] Université Cadi Ayyad, Faculté des Sciences et Techniques-Gueliz, Département Sciences de la Terre, Avenue Abdelkrim el Khattabi, BP 549, 40000 Marrakech, Morocco
* Corresponding author: Fabienne.Giraud-Guillot@univ-grenoble-alpes.fr

www.borntraeger-cramer.de
DOI: 10.1127/nos/2020/0603 0078-0421/2020/0603 $ 9.00

2005, Jaillard et al. 2013, 2017), (3) a rich endemic ammonite fauna (e. g. Pervinquière 1907, Douvillé 1916, Moret and Mahmoud 1953, Dubourdieu 1956, Latil 2011, Robert in Peybernes et al. 2013, Luber et al. 2017, 2019) and (4) deposition of organic-rich sediments in Tunisia (Heldt et al. 2008, Elkhazri et al. 2009, 2013, Ben Fadhel et al. 2011, 2014, Godet et al. 2014). This time interval is poorly understood because of frequent sedimentary hiatuses and endemic fauna. Additionally, the upper Aptian–lower Albian transgression is poorly documented, because of the thick, monotonous and fossil-poor clay succession that represents most of the Albian stage.

The Essaouira-Agadir Basin (EAB) presents numerous, well-exposed, accessible and fossiliferous outcrops of the Lower Cretaceous series. Therefore, it provides an excellent opportunity to calibrate different stratigraphic records. Recently, based on a multi-disciplinary research, Luber et al. (2017, 2019) proposed a chronostratigraphic framework for the Aptian. However, their few selected sections are often condensed and/or incomplete, and their proposed biostratigraphic framework is therefore debatable.

Following the works by Peybernes et al. (2013) and Jaillard et al. (2019a), the aim of this study was thus to establish an integrated stratigraphic framework of the latest Barremian–early Albian interval in the EAB. We focused on (i) the identification of sedimentary discontinuities, (ii) a high-resolution ammonite and calcareous nannofossil biostratigraphy, and (iii) carbon isotope ($\delta^{13}C$ values) stratigraphy. Here we document the record of the Aptian–Albian boundary in various Tethyan settings and it is discussed considering the recent proposed Global Boundary Stratotype Section and Point (GSSP) for the base of the Albian stage of the Col de Pré-Guittard section (Vocontian Basin, northern Tethyan margin; Kennedy et al. 2017).

2. Geological setting of the Essaouira-Agadir Basin

The Essaouira-Agadir Basin (EAB) is located in the Western High Atlas of Morocco (Fig. 1). The EAB is part of the African passive margin of the Central Atlantic Ocean, which was part of the Mesozoic Tethyan Ocean (Stets and Wurster 1982, Zühlke et al. 2004, Hafid et al. 2008). Atlantic rifting started in the Late Permian–Triassic, and culminated with oceanic crust accretion in the early Middle Jurassic (Hafid et al. 2000, Le Roy and Piqué 2001, Gouiza 2011). The syn-rifting stage gave way to the deposition of thick clastic red bed deposits of Late Permian-Triassic age, overlain by a thick series of shales and evaporites intercalated with tholeiitic basaltic flows dated as Early Jurassic (Medina 1994, 1995, Hafid et al. 2000, Davison 2005). Following the appearance of oceanic crust, the post-rift stage (Middle Jurassic to Early Cretaceous) was characterized by thermal subsidence of the margin (Medina 1994, Gouiza 2011, Bouatmani et al. 2007). This, combined with eustatic transgressions (Le Roy et al. 1998) gave way to the development of a widespread, shallow marine carbonate platform (Zühlke et al. 2004, Davison 2005, Hafid et al. 2008). The sharp regression of latest Jurassic age is followed by the Cretaceous transgression (Zühlke et al. 2004). The latter is interrupted by significant regressions within Valanginian, (Rey et al. 1988, Masrour et al. 2004), late early Hauterivian and latest Barremian-earliest Aptian times (Canérot et al. 1986, Witam 1998, Ferry et al. 2007, Jaillard et al. 2019b). The lower Aptian transgression led to the deposition of shelf limestones grading upwards into open marine shales of late Aptian to Albian age, capped by shallow marine limestones and sandstones of latest Albian age (Wiedmann et al. 1978, Butt 1982, Ettachfini 1992). The upper Cretaceous transgression is then characterized by two major regressive periods of late Cenomanian (Ettachfini et al. 2005, Jati et al. 2010, Essafraoui et al. 2015), and Senonian age (Algouti et al. 1999), respectively.

Salt tectonics and diapir activity began in the Jurassic and occurred repeatedly during the Cretaceous, controlling facies distribution mainly in the distal, offshore part of the basin (Mehdi et al. 2004, Zühlke et al. 2004, Tari and Jabour 2013). Compressional deformation began in the Late Cretaceous, provoked the emergence of the EAB in the Paleocene and culminated in Late Eocene-Pliocene times with the Atlas orogeny (Frizon de Lamotte et al. 2000, 2008), which folded the sedimentary pile of the EAB.

In the study area, three East-West trending folds can be distinguished: (1) a central, gentle synclinorium dipping westward, (2) the northern Amsitene anticline, and (3) the southern Cap Rhir-Anklout anticline (Fig. 1). These E-W folds define three areas in the EAB: the northern (Essaouira), central (Tamanar), and southern (Agadir) areas (Fig. 1). The present work was focused on the two latter areas.

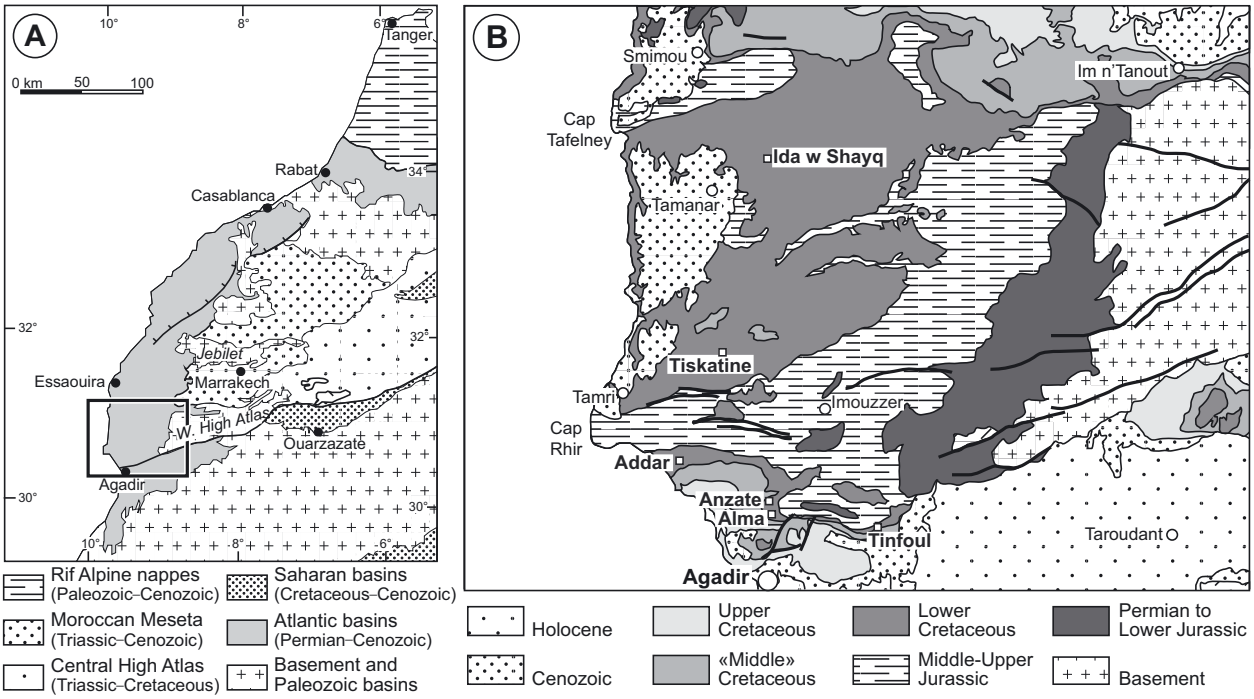

Fig. 1. Location of the study area. A. Location of the Essaouira-Agadir basin. B. Geological sketch of the EAB, and location of the studied sections (white square).

3. Lithostratigraphy and correlation of the studied sections

In the EAB, the Aptian strata usually rest on sandy limestone or dolostone (Bouzergoun Formation), of latest Barremian age (Jaillard et al. 2019b). Sections begin with a thin series of argillaceous limestones interbedded with marlstones of early Aptian–early late Aptian. They progressively grade upward into a mostly marly succession of late Aptian age (Peybernes et al. 2013). These deposits roughly coincide with the 15 to 30 m thick Tamzergout Formation (Witam 1998, Luber et al. 2017). The overlying series of Albian age (Witam 1998, Oued Tidzi Formation) is underlined by a noticeable bed of yellow dolomitic sandstone. Its lower part comprises a mainly argillaceous marl series (15–35 m), overlain by alternating argillaceous marlstones and yellow dolomitic sandstone beds (25–35 m; *Beudanticeras* beds" of Ambroggi (1963)). Above is a thick series of monotonous, argillaceous marlstones, with scarce limestone or sandstone beds.

A detailed sedimentological analysis allowed identifying seven main discontinuity surfaces in this succession, labeled D0 to D6, and defining at least seven depositional sequences. D0 corresponds to a karsted surface, usually located at the top of the Bouzergoun Formation. D1 is also a karsted surface, generally amalgamated with D0. In some sites, however, it forms a distinct surface that may be correlated with the beds rich in "*Cheloniceras* ammonites". D2 has not been identified confidently in all sections, especially in the South, where D2 is difficult to differentiate from D1. When present, it is marked by a limestone bed containing phosphatized ammonites and other fossils, located a few decimeters above the bed rich in "*Tropaeum* ammonites", or on top of it (e. g. Ida w Shayq, Tiskatine). D2 is thought to materialize a submarine hiatus. D3 is a submarine erosional surface located a few decimeters above the bed rich in "*Nolani* ammonites" (e. g. Addar, Anzate, Tiskatine), or directly on top of it (e. g. Alma, Ida w Shayq), depending on the amount of erosion that occurred during the submarine hiatus. D4 is well marked at the base of a conspicuous yellow dolomitic sandstone bed that marks the base of the Oued Tidzi Formation. It is an erosional surface, which may have removed parts of the underlying argillaceous marlstones, the thickness of which is highly variable (7 to 17 m). Therefore, D4 represents

a sedimentary hiatus. Although no criteria of emergence have been found below D4, probably because of the argillaceous nature of the underlying deposits, an emergence period is likely. D5 is a probably marine, erosional surface at the base of the alternating succession of yellow sandstone beds and argillaceous interbeds ("*Beudanticeras* beds"). Finally, D6 is an erosional surface at the base of thick sandstone beds, located close to the top of the "*Beudanticeras* beds", and below a thick series of argillaceous marlstones.

These discontinuity surfaces, interpreted as sequence boundaries, make possible correlations throughout the EAB, confirmed by the ammonite fauna.

4. Material and methods

Six sections located along two transects, oriented east-west and south-north, respectively, were selected for biostratigraphic and carbon stable isotope studies (Fig. 1). The sections are named Addar, Alma, Anzate, Ida w Shayq, Tinfoul and Tiskatine, and their geographic coordinates can be found in Jaillard et al. (2019a).

4.1. Ammonite sampling

The bed-by-bed sampling of ammonites was carried out in 141 levels from the six sections. This material is part of an important biostratigraphic regional study, based on the analysis of thousands of specimens collected in the six sections described here, and in seven other sections of the EAB in the years 2008 and 2017. A detailed ammonite distribution of the Addar section was already presented in Peybernes et al. (2013). New collected material changed some of our biostratigraphic calibration, as explained below.

Identifications were based on comparisons with Moroccan collections (Kilian and Gentil 1906, 1907, Roch 1930, Ambroggi and Breistroffer 1959), with focus on original specimens and plaster casts of the type series. We also integrate the study of specimens from southern and northern Tethyan provinces deposited in the French universities and museums (D'Orbigny, Fallot, Busnardo and Atrops Collections). Detailed paleontological descriptions and discussions will be presented in a forthcoming publication.

4.2. Ammonite zonation

Aptian to lower Albian ammonite associations are known since Brives (1905), Lemoine (1905), Gentil (1905) and Kilian and Gentil (1906). Additional faunal lists were provided by Roch (1930), Ambroggi and Breistroffer (1959), Ambroggi (1963), Wiedmann et al. (1978, 1982), Rey et al. (1986, 1988) and Witam (1998). A first revision of the regional biostratigraphic framework was made by E. Robert (*in* Peybernes et al. 2013). Calibration with the ammonite standard zonation was proposed since numerous Tethyan species were identified, among them the index-species *Deshayesites deshayesi* and *Epicheloniceras martini*. Conversely, Luber et al. (2017, 2019) introduced eight regional zones and subzones for the same interval, because of the non-recognition of index-species of the Tethyan standard. Ammonite populations of the EAB are indeed characterized by a high provincialism (Peybernes et al. 2013, Luber et al. 2017, 2019). Endemic new species were identified and listed in the present study, especially for Acanthohoplitids.

Since the publication by Kennedy et al. (2017), the Global boundary Stratotype Section and Point (GSSP) of the Albian Stage is defined by the first occurrence (FO) of the planktonic foraminifera *Microhedbergella renilaevis* at meter 37.4 of the Col de Pré-Guittard section (Drôme, France). In this locality, the first Albian ammonites, considered as a secondary marker, occur 30.6 meters above, at the base of the "Niveau Paquier", a condensed level. This results in a difficult identification of the Aptian–Albian boundary with ammonites. Moreover, even if Kennedy et al. (2017) are considering the boreal species *Leymeriella (Leymeriella) tardefurcata* as a useful proxy, it cannot be used at a global scale, especially in the southern Tethyan margin. Consequently, we consider the GSSP of the Albian stage as problematic and little appropriate. In practice, in the EAB, we used the FO of the genera *Douvilleiceras*, *Oxytropidoceras*, *Parengonoceras* and/or *Parabrancoceras* as a marker of the Albian stage. Our sections can be considered as references for the Aptian–Albian ammonite succession of northwest Africa: Ida w Shayq for the latest Barremian to early Aptian interval and the Aptian–Albian boundary, Tiskatine and Addar for the latest Aptian to early Albian interval.

4.3. Calcareous nannofossils

One hundred and seventy-six samples, selected from argillaceous marlstone to limestone and collected in the six studied sections, were investigated for calcareous nannofossil quantitative analysis (Peybernes et al. 2013, Hassanein 2016, Jaillard et al. 2019a). Smear

slides were prepared using the random settling technique of Geisen et al. (1999), a method adapted from Beaufort (1991). It allows calculating absolute abundances of calcareous nannofossils. Additionally, 37 smear slides were prepared from samples collected in the Addar, Alma and Anzate sections, but only semi-quantitative analyses were performed. Nannofossils were observed using a light polarizing microscope, at 1000 X magnification. The observation of marker species has been achieved in all smear slides by counting from 5 to 7 and 6 to 13 longitudinal transverses (200 fields of view), in the richest and poorest samples, respectively. The taxonomic frameworks of Perch-Nielsen (1985), Bown et al. (1998), and Nannotax3 (Young et al. 2017) were followed. For nannoconids, the work of Deres and Achéritéguy (1980) was followed. Nannofossil preservation was evaluated following the classes defined by Roth (1983).

4.4. Calcareous nannofossil zonation

The calcareous nannofossil zones and subzones applied to the investigated sections are the NC zones of Bralower (1987), Bralower et al. (1993 1995), modified from Roth (1978). This zonation scheme was selected as a result of its applicability to low-latitude Tethyan continental margins (Bralower et al. 1993). We will discuss the applicability of this zonal scheme in the Essaouira-Agadir Basin sections. Numerous markers used in this scheme have been recognized in deep-sea sections, and are often difficult to find in onshore sections. In addition to nannofossil zones, we used secondary bioevents.

4.4.1. The case of the calcareous nannofossil *Rhagodiscus angustus* Zone (NC7)

The NC7 Zone was defined as the interval between the FO of *Eprolithus floralis* and the FO of *Prediscosphaera columnata*. It was subdivided into three subzones, called respectively A, B, and C (Bralower et al. 1993). The NC7A Subzone was defined as the interval between the FO of *E. floralis* and the last occurrence (LO) of *Micrantholithus* spp. (including both *M. hoschulzii* and *M. obtusus*). The NC7B Subzone was defined as the interval between the LO of *Micrantholithus* spp. and the FO of *Rhagodiscus achlyostaurion*. The NC7C was defined as the interval between the FO of *R. achlyostaurion* and the FO of *Prediscosphaera columnata*. However, Bralower et al. (1993) mentioned that the events they used to define the three subzones are problematical. Luber et al. (2019) mentioned that the standard Aptian nannofossil subzonal scheme needs revision. As a result, in the first stage, we present only occurrence of nannofossil taxa used to define the three subzonal units if recognized, without applying NC7 subzonal subdivisions. We then discuss the subzonal scheme of Bralower et al. (1993) and propose a new one for the NC7 Zone.

4.4.2. Stratigraphic significance of morphological variations within two marker genera: *Prediscosphaera* and *Hayesites*

Prediscosphaera columnata and *Hayesites albiensis* are widely distributed in the Boreal and Tethyan Realms, in DSDP, ODP and IODP sites and were considered as stratigraphic markers. However, transitional forms between these species were recognized (Bown 2005, Bown, in Kennedy et al. 2000, 2014, Mutterlose et al. 2003), and need to be discussed further. Morphological variations within the *Prediscosphaera* and *Hayesites* genera have been investigated in the present study.

4.5. Stable isotopes

Stable carbon and oxygen isotope analysis were performed on 230 whole rock samples at the stable isotope laboratories of the Institute of Earth Surface Dynamics of the University of Lausanne, using a Thermo Fisher Scientific Gas Bench II carbonate preparation device connected to a Delta Plus XL isotope ratio mass spectrometer (IRMS; Révész and Landwehr 2001). The CO_2 extraction was done at 70 °C. The stable carbon and oxygen isotope ratios were reported in the delta (δ) notation as the per mil (‰) relative to the Vienna Pee Dee belemnite standard (VPDB), where $\delta = (R_{sample} - R_{standard})/R_{standard} \times 1000$ and $R = \delta^{13}C/^{12}C$ or $^{18}O/^{16}O$. The $\delta^{13}C_{carb}$ and $\delta^{18}O_{carb}$ values were standardized relative to the international VPDB scale by calibration of the reference gases and working standards with international reference materials NBS 18 (carbonatite, $\delta^{13}C = -5.04$ ‰, $\delta^{18}O = -23.00$ ‰) and NBS 19 (limestone, $\delta^{13}C = +1.95$ ‰, $\delta^{18}O = -2.19$ ‰). Analytical uncertainty (1 sigma), monitored by replicate analyses of the international calcite standard NBS 19 and the laboratory standard Carrara Marble ($\delta^{13}C = +2.05$ ‰, $\delta^{18}O = -1.7$ ‰) was not greater than ±0.05‰ for $\delta^{13}C$ and ±0.1‰ for $\delta^{18}O$. The $\delta^{13}C_{carb}$ and $\delta^{18}O_{carb}$ results are presented in Supplementary Information.

5. Results

5.1. Ammonite biostratigraphy

Abundance and diversity are highly uneven throughout the successions. Rich horizons are found in the lowermost Aptian, basal upper Aptian, uppermost Aptian and basal Albian strata. The preservation of specimens ranges from pyritic and phosphatic molds, especially for the latest Aptian and lowermost Albian deposits, to internal calcareous molds, unfortunately frequently fragmented, crushed and incomplete.

Sections of the northern area provided rich ammonite successions for the early Aptian, while sections of the central and southern areas yielded rich associations for the late Aptian and early Albian intervals. Ammonite assemblages are largely dominated by Douvilleiceratids, Acanthohoplitids and Desmoceratids, associated with Ancyloceratids, Phylloceratids and Tetragonitids. Mediterranean ammonite standard zones (Reboulet et al. 2018) are identified for the latest Barremian–earliest late Aptian interval.

Ammonite index taxa are illustrated in Plates 1, 2 and 3. Representative ammonite associations are listed in Table 1 and the distribution of the species is presented for each section (Figs. 2 to 6), except for Addar, already illustrated in Peybernes et al. (2013), for which only actualized data are presented.

5.1.1. Martelites sarasini ammonite Zone

The latest Barremian zone is only recognized in Ida w Shayq (Fig. 2), with the occurrence of *Kutatissites* sp. and *Pseudocrioceras* sp.

5.1.2. Deshayesites forbesi ammonite Zone

In the EAB, the early Aptian is represented by low diversified assemblages, enriched in condensed layers and sedimentary hiatuses. The Barremian–Aptian boundary and the *Deshayesites oglanlensis* Zone were not recognized. The *D. forbesi* Zone is only identified in Ida w Shayq (Fig. 2) and Tiskatine (Fig. 3a). Its base is defined by the FO of *Cheloniceras cornuelianum* (Plate 1.1–1.4) or of the genus *Prochelonicera*s sp.

5.1.3. Deshayesites deshayesi ammonite Zone

The *Deshayesites deshayesi* Zone is recognized in Ida w Shayq, Tiskatine and Alma. Its base is defined by the FO of the index-species or of first evolved *Cheloniceras*, as *C. meyendorfi* (Plate 1.5–1.6) in Ida w Shayq (Fig. 2), and of *Cheloniceras* sp. in Alma (Fig. 5). Cheloniceratids largely dominate the assemblage and Ancyloceratids are common representatives of the zone (Table 1). In Alma, a condensed level, overlying discontinuities D1-2, yielded an association characterizing the *D. deshayesi* to *Epicheloniceras martini* zones. It includes *Deshayesites deshayesi*, *Dufrenoyia* cf. *furcata* (Plate 1.7–1.8), *Colombiceras crassicostatum*, and *Epicheloniceras martini*.

5.1.4. Dufrenoyia furcata ammonite Zone

The *Dufrenoyia furcata* Zone has been tentatively recognized in Ida w Shayq and Tiskatine sections. Its base is mainly defined by the FO of the index-species or evolved forms of *Deshayesites*, like *D. consobrinoides* (Plate 1.9–1.10). In Tiskatine (Fig. 3a), the first level above the discontinuity D1 yielded an association characterizing both the *D. furcata* and *Epicheloniceras martini* zones. This association includes *Pseudohaploceras angladei*, *Colombiceras* cf. *crassicostatum* (Plate 1.13–1.14) or *Epicheloniceras* gr. *gracile-debile* (Plate 1.11–1.12).

5.1.5. Epicheloniceras martini ammonite Zone

The zone is represented in the whole EAB, except in its eastern part. However, the ammonite fauna is moderately diversified. The base of the zone is defined by the FO of the index-species, of first *Colombiceras* and of endemic *Neodufrenoyia*. Its base is hypothetically placed at the FO of *Australiceras* sp. in Ida w Shayq (Fig. 2). Associated to endemic *Neodufrenoyia* nov. sp. 1, the assemblage of the zone is dominated by *Colombiceras* cf. *discoidale*, *Pseudoaustraliceras* cf. *hirtzi* (Plate 2.1) and *Australiceras* cf. *carinatoverrucosum* (Table 1). Revising the work by Peybernes et al. (2013), the first level of the Addar section is now ascribed to the *E. martini* Zone.

5.1.6. Parahoplites melchioris ammonite Zone

The base of the zone is not characterized and its position is uncertain in most sections, because of very scarce and poorly-preserved specimens. We hypothetically place its base at the first appearance of *Elsaisabellia* sp. in Ida w Shayq (Fig. 2) and Tiskatine (Fig. 3a), or the occurrence of *Acanthohoplites bigoureti anthulai* (Plate 1.18–1.19) and *Epicheloniceras* sp. in Anzate (Fig. 4). We are unable to characterize this zone in other sections.

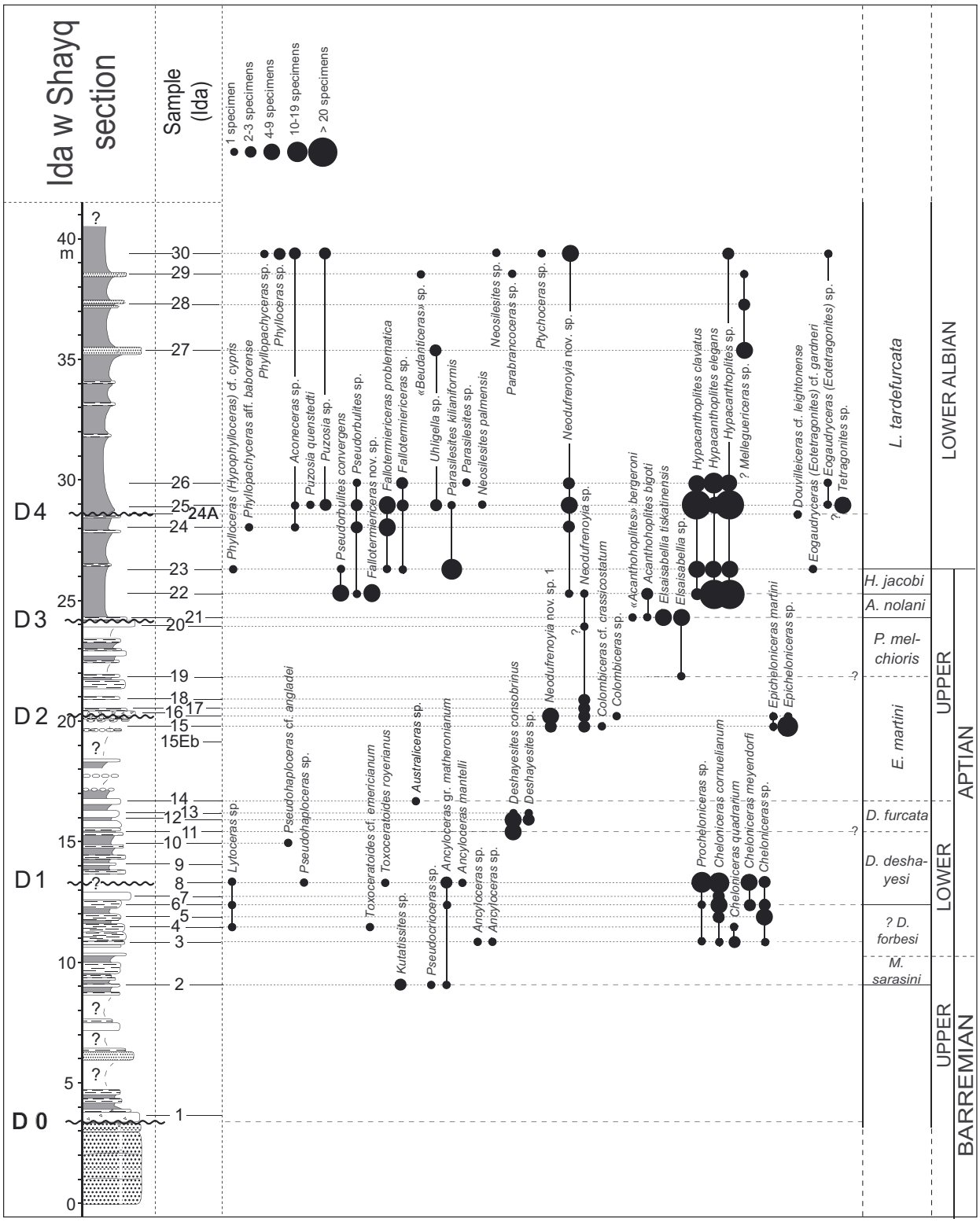

Fig. 2. Ida w Shayq section. Ammonite distribution and standard stratigraphic calibration.

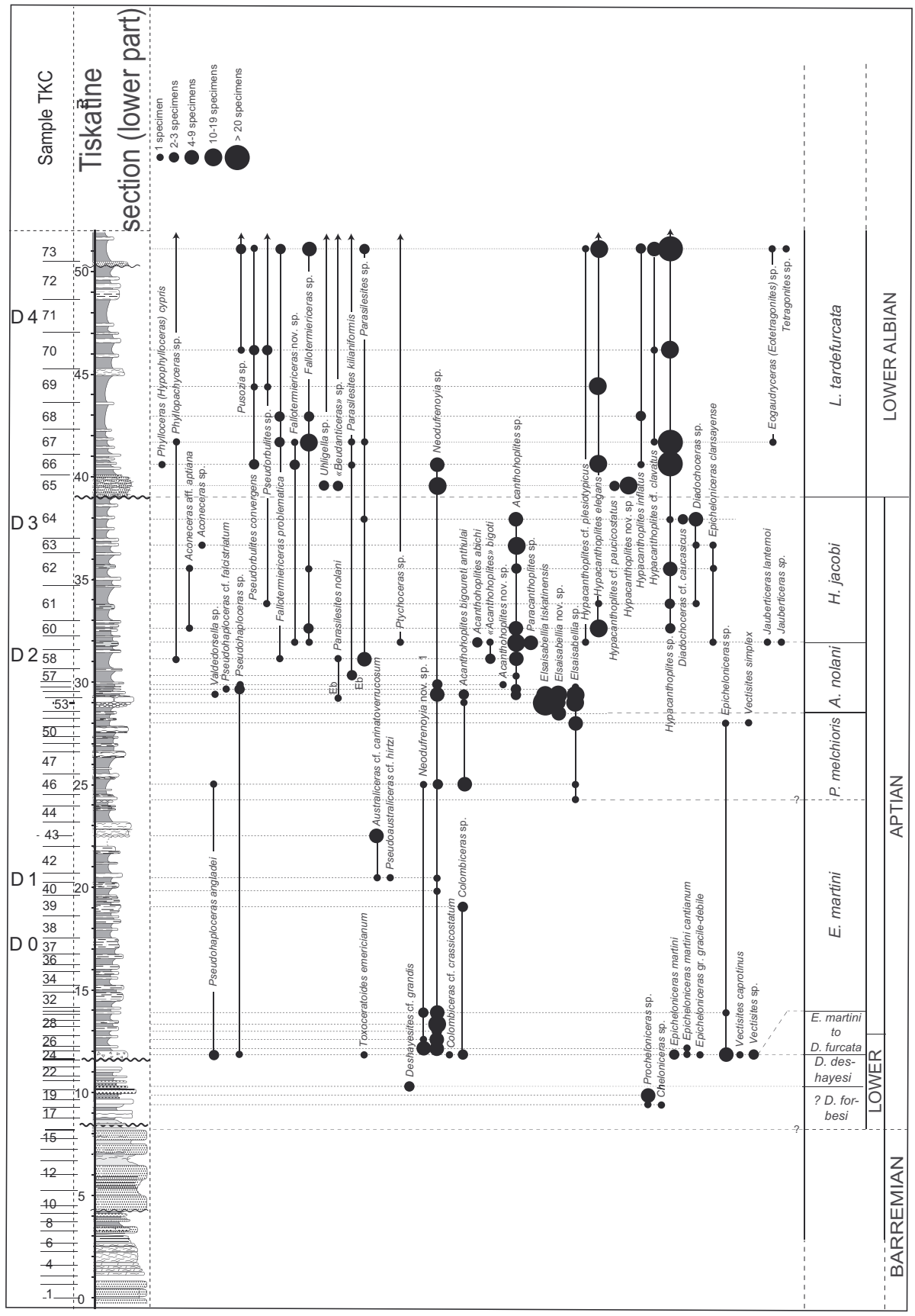

Fig. 3a. Tiskatine, lower series, section. Ammonite distribution and standard stratigraphic calibration.

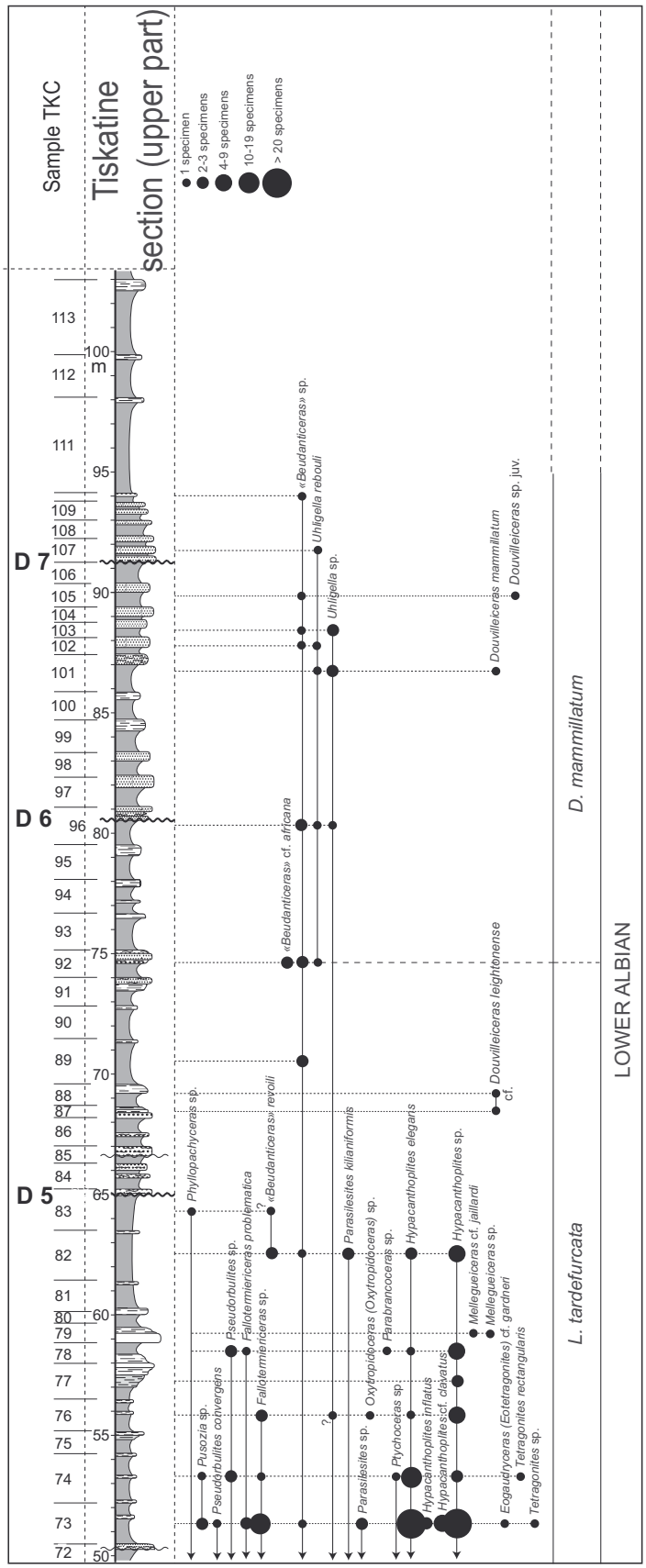

Fig. 3b. Tiskatine, upper series, section. Ammonite distribution and standard stratigraphic calibration.

Table 1. Representative ammonite assocations of the EAB, and correlations with the lower Aptian to lower Albian Standard Ammonite zones.

Substages	Ammonite standard zones	Ammonite associations
Early Albian	*Douvilleiceras mammillatum*	*Douvilleiceras mammillatum* (Schlotheim), *"Beudanticeras"* cf. *africana* Pervinquière, *Uhligella rebouli* Jacob, *Parengonoceras hachourii* (Breistroffer *in* Dubourdieu)
	Leymeriella tardefurcata	*Phylloceras (Hypophylloceras)* cf. *cypris* Fallot & Termier, *Phyllopachyceras* aff. *baborense* (Coquand), *Puzosia quenstedti* (Parona & Bonarelli), *Pseudorbulites convergens* (Jacob), *Fallotermiericeras problematica* (Fallot et Termier), *"Beudanticeras" revoili* (Pervinquière), *Parasilesites kilianiformis* (Fallot), *Neosilesites palmensis* (Fallot & Termier), *Oxytropidoceras* sp., *Parabrancoceras* sp., *Ptychoceras* sp., *Parengonoceras* cf. *bassei* (Bataller), *Hypacanthoplites elegans* (Fritel), *Hypacanthoplites clavatus (*Fritel), *Hypacanthoplites* cf. *paucicostatus* (Breistroffer in Dubourdieu), *Mellegueiceras jaillardi* Latil, *Douvilleiceras leightonense* Casey, *Eogaudryceras (Eotetragonites)* cf. *gardneri* (Murphy), *Tetragonites rectangularis* (Wiedmann)
Late Aptian	*Hypacanthoplites jacobi*	*Pseudorbulites convergens* (Jacob), *Aconeceras aptiana* (Sarasin), *Fallotermiericeras problematica* (Fallot et Termier), *Ptychoceras* sp., *Hypacanthoplites elegans* (Fritel), *Hypacanthoplites clavatus* (Fritel), *Diadochoceras caucasicus* (Luppov), *Diadochoceras migneni* (Seunes), *Epicheloniceras clansayense* (Jacob), *Jauberticeras lanternoi* Wiedmann, *Eogaudryceras (Eotetragonites)* sp.
	Acanthohoplites nolani	*Elsaisabellia tiskatinensis* (Luber et al.), *Fallotermiericeras* sp., *Acanthohoplites bigoureti* (Seunes), *Acanthohoplites bergeroni* (Seunes), *"Acanthohoplites" bigoti* (Seunes), *Protacanthoplites bogdanovae* (Tovbina), *Diadochoceras* sp., *Epicheloniceras clansayense* (Jacob)
	Parahoplites melchioris	*Acanthohoplites bigoureti anthulai* Breistroffer, *Elsaisabellia* sp., *Epicheloniceras* sp.
	Epicheloniceras martini	*Epicheloniceras martini* (d'Orbigny), *Epicheloniceras* gr. *gracile-debile* (Casey), *Pseudoaustraliceras* cf. *hirtzi* Collignon, *Australiceras* cf. *carinatoverrucosum* (Sinzow), *Dufrenoyia* gr. *dufrenoyi* d'Orbigny, *Neodufrenoyia* nov. sp. 1, *Colombiceras crassicostatum* (d'Orbigny)
Early Aptian	*Dufrenoyia furcata*	*Dufrenoyia furcata* (Sowerby), *Deshayesites consobrinoides* (Sinzow)
	Deshayesites deshayesi	*Deshayesites deshayesi* (d'Orbigny in Leymerie), *Deshayesites* cf. *grandis* (Spath), *Paracheloniceras* sp., *Cheloniceras cornuelianum* (d'Orbigny), *Cheloniceras meyendorfi* (d'Orbigny), *Ancyloceras mantelli* Casey, *Ancyloceras* gr. *matheronianum* (d'Orbigny)
	Deshayesites forbesi	*Prochelonicera*s sp., *Cheloniceras cornuelianum* (d'Orbigny), *Cheloniceras quadratum* (Spath), *Ancyloceras* sp.

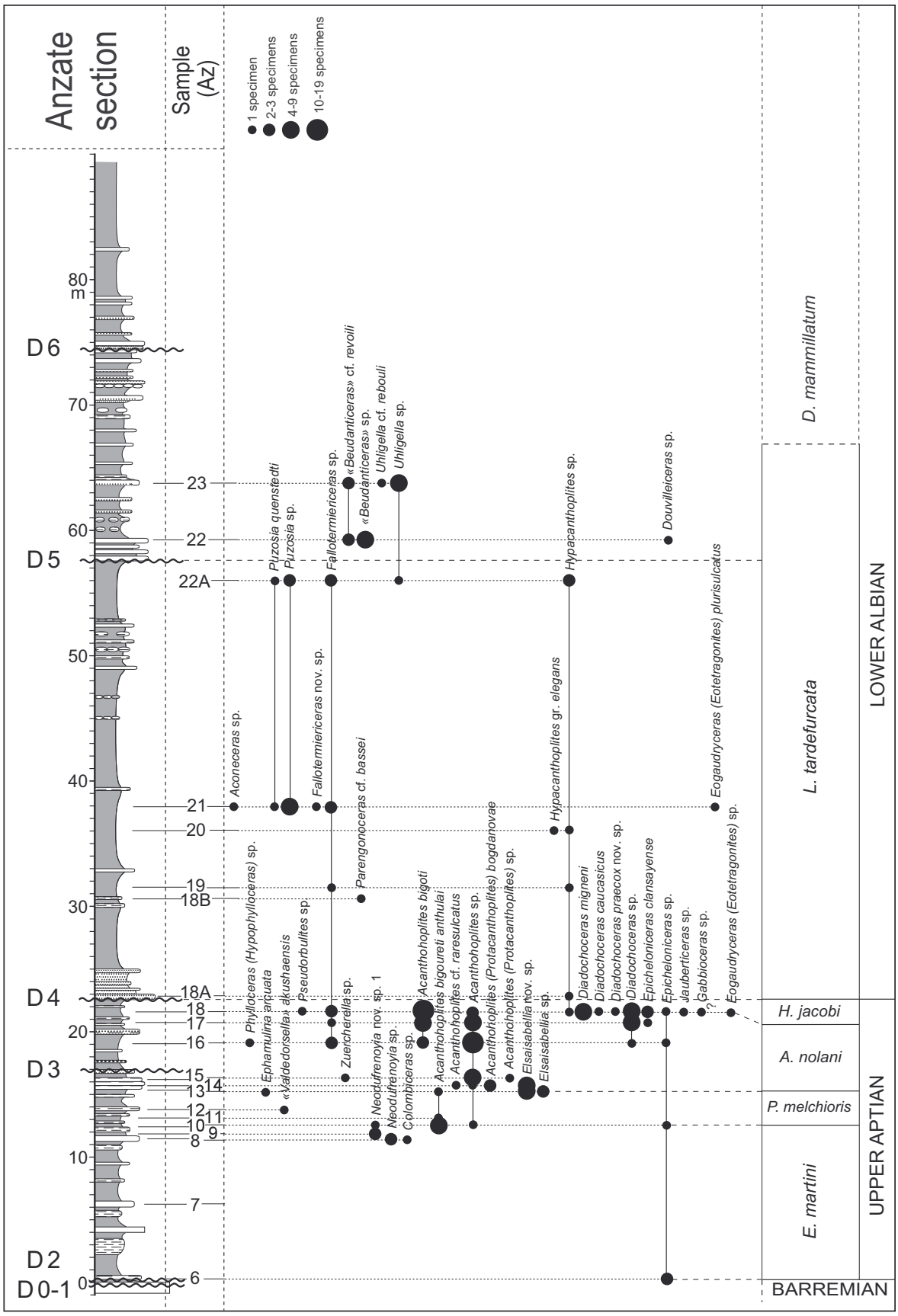

Fig. 4. Anzate section. Ammonite distribution and standard stratigraphic calibration.

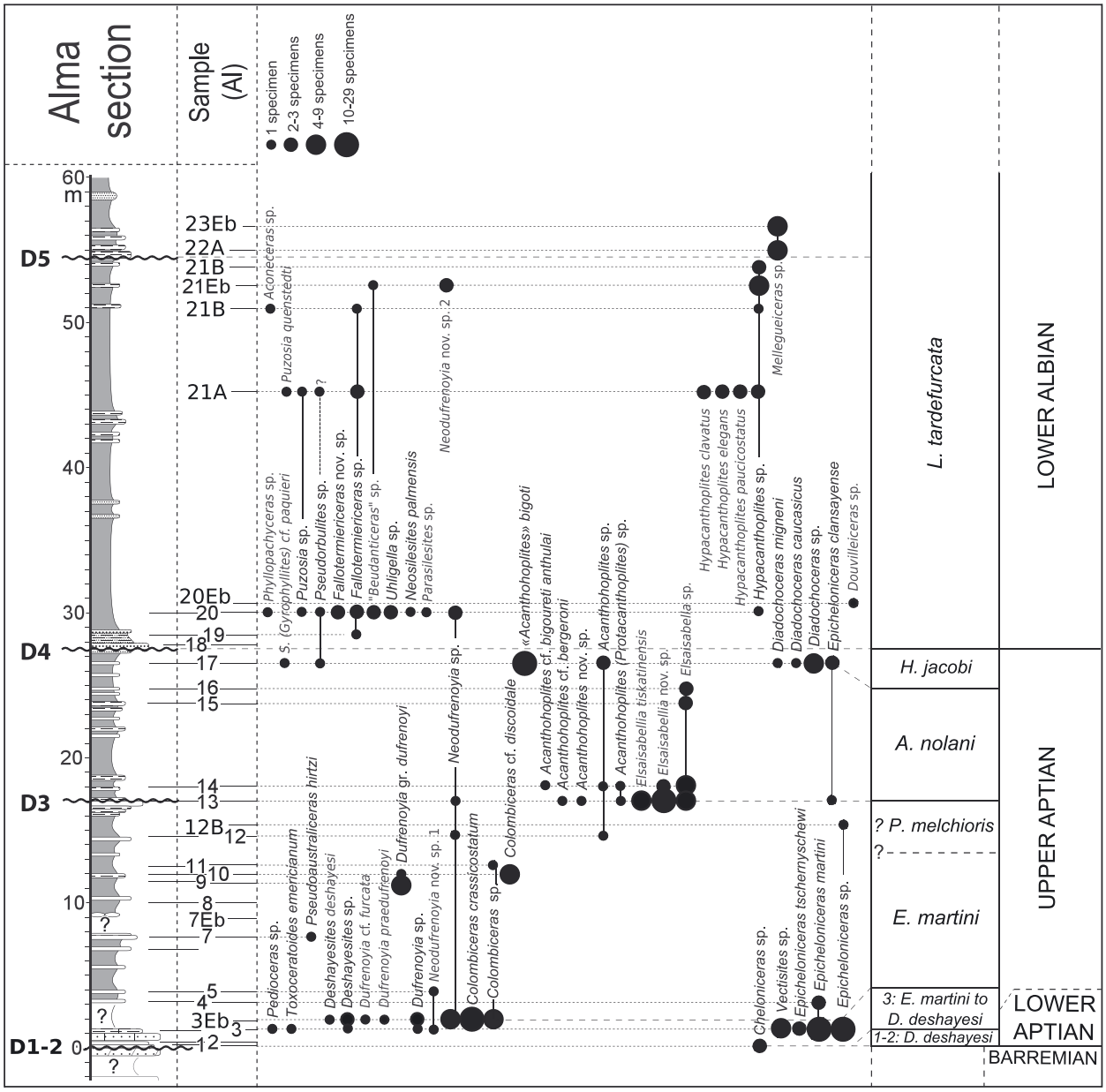

Fig. 5. Alma section. Ammonite distribution and standard stratigraphic calibration.

5.1.7. Acanthohoplites nolani ammonite Zone

The zone is characterized by diversified ammonite associations (Table 1), observed in the whole EAB and referred to as the "Nolani bed" by Ambroggi (1963). Its base is defined by the FO of the index-species that represents a large percentage of the fauna, and of *Epicheloniceras clansayense* or *Elsaisabellia tiskatinensis* (Plate 2.2–2.3). The genera *Elsaisabellia (E. tiskatinensis, Elsaisabellia* nov. sp.) and *Acanthohoplites* (*A. bergeroni*, *A. bigoureti anthulai, "A." bigoti*) dominate the assemblage of the zone. Phylloceratids, associated with *Parasilesites* sp., *Protacanthoplites bogdanovae* (Plate 1.20–1.21), *Diadochoceras* sp. and *Epicheloniceras clansayense* (Plate 1.17), are minor representatives. In Tinfoul (Fig. 6), the lowermost succession yielded scarce and poorly preserved ammonites. The early Aptian to earliest late Aptian interval is not identified. Biostratigraphic calibration must be taken with caution. The level containing the discontinuity D3 is assigned to the *A. nolani* to *Hypacanthoplites jacobi* zones interval.

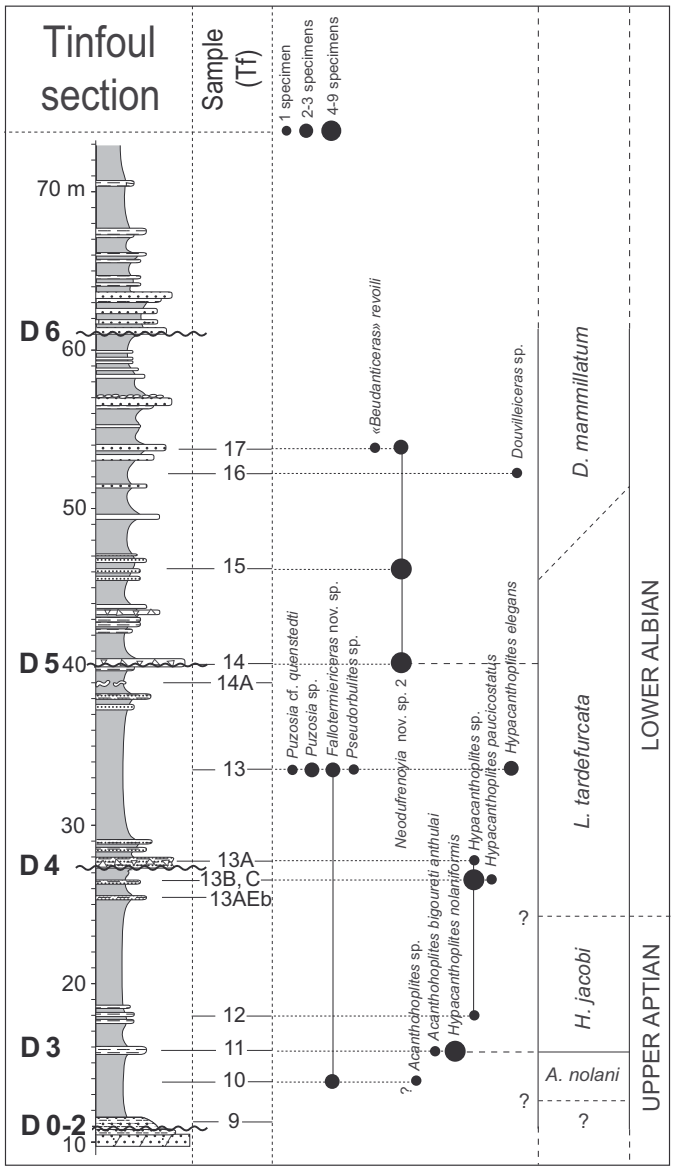

Fig. 6. Tinfoul section. Ammonite distribution and standard stratigraphic calibration.

5.1.8. Hypacanthoplites jacobi ammonite Zone

The lower part of the *Hypacanthoplites jacobi* Zone is recognized in all sections while its upper part is usually removed by the erosion related to discontinuity D4. The *z*one is characterized by highly diversified ammonite associations (Table 1). Its base is defined by the FO of *Pseudorbulites convergens* and first representatives of *Hypacanthoplites* and *Diadochoceras*. It is restricted to one level in Ida w Shayq, Anzate and Alma. The assemblage is dominated by *Hypacanthoplites* (*H. clavatus* (Plate 2.18–2.20), *H. elegans* (Plate 2.21–2.22), *Fallotermiericeras problematica* (Plate 2.23–2.25) and *Pseudorbulites convergens* (Plate 2.8–2.10). The association is completed by Tetragonitids, *Epicheloniceras clansayense* (Plate 1.15–1.16), *Aconeceras* aff. *aptiana* and *Diadochoceras* including *D. caucasicus* (Plate 2.4–2.5) and *Diadochoceras migneni.* In Addar (Peybernes et al. 2013), the base of the zone is moved up to the FO of *Hypacanthoplites*.

5.1.9. Leymeriella tardefurcata ammonite Zone

The ammonite fauna remains diversified during basal Albian times. The lower part of the *Leymeriella tarde-*

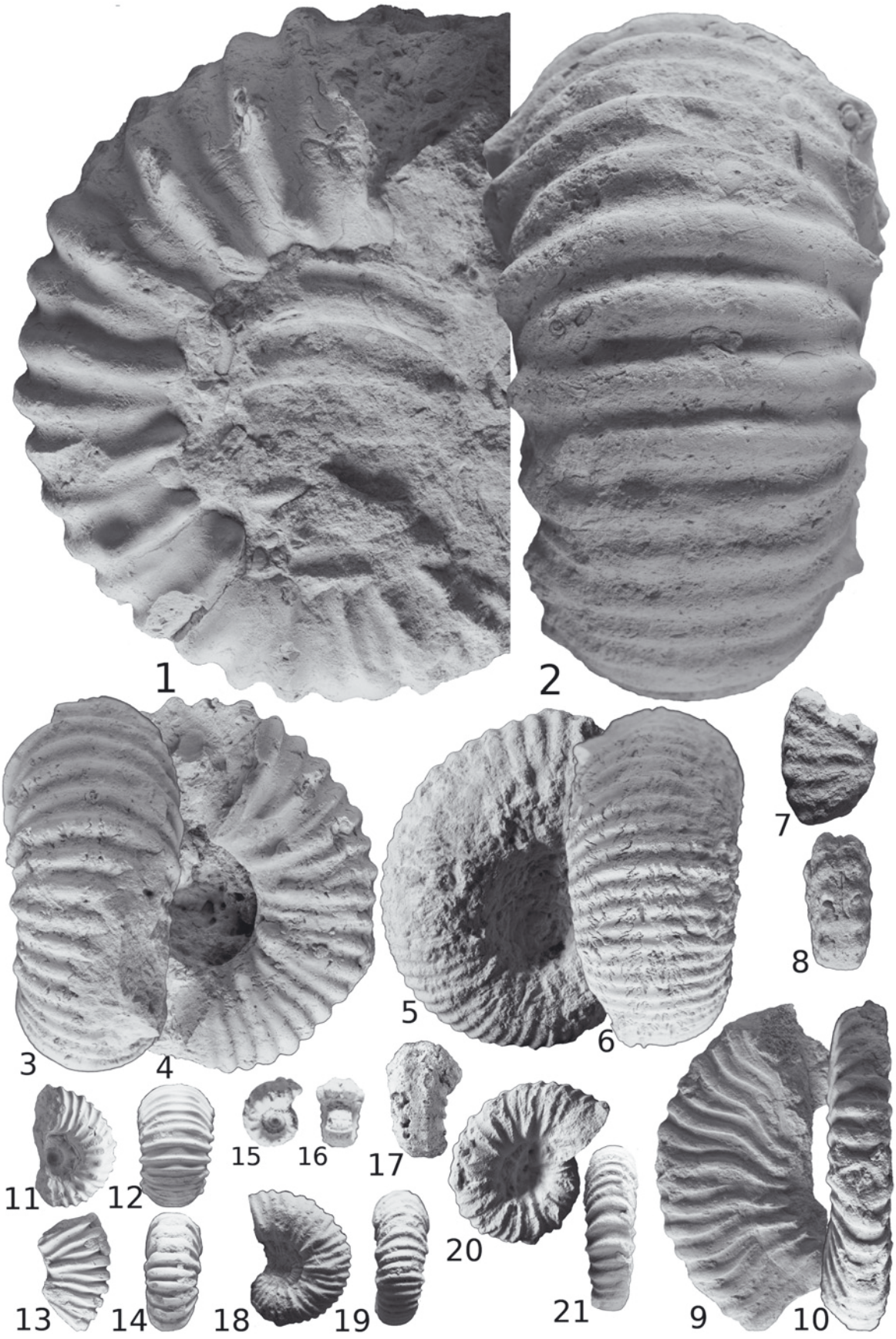
1
2
3
4
5
6
7
8
9
10
11
12
13
14
15
16
17
18
19
20
21

Plate 1. (1–2) *Cheloniceras cornuelianum* (d'Orbigny, 1841), UJF-ID.12231, Ida w Shayq section (IDA-8), *Deshayesites forbesi* Zone, early Aptian; (3–4) *Cheloniceras cornuelianum* (d'Orbigny, 1841), UJF-ID.12232, Ida w Shayq section (IDA-8), *Deshayesites forbesi* Zone, early Aptian; (5–6) *Cheloniceras meyendorfi* (d'Orbigny, 1845), UJF-ID.12233, Ida w Shayq section (IDA-8), *Deshayesites deshayesi* Zone, early Aptian; (7–8) *Dufrenoyia furcata* (Sowerby, 1836), UJF-ID.12234, Alma section (AL-3), *Dufrenoyia furcata* Zone, early Aptian; (9–10) *Deshayesites consobrinoides* (Sinzow, 1898), UJF-ID.12235, Ida w Shayq section (IDA-11), *Dufrenoyia furcata* Zone, early Aptian; (11–12) *Epicheloniceras* gr. *gracile-debile* Casey (1961), UJF-ID.12236, Tiskatine section (TKC-24), *Epicheloniceras martini* Zone, Late Aptian; (13–14) *Colombiceras crassicostatum* (d'Orbigny, 1841), UJF-ID.12237, Tiskatine Center section (TKC-21), *Epicheloniceras martini* Zone, late Aptian; (15–16) *Epicheloniceras clansayense* (Jacob, 1905), UJF-ID.12238, Tiskatine section (TKC-62), *Acanthohoplites nolani to Hypacanthoplites jacobi* Zone, late Aptian; (17) *Epicheloniceras clansayense* (Jacob, 1905), UJF-ID.12239, Alma section (AL-15), *Acanthohoplites nolani to Hypacanthoplites jacobi* Zone, late Aptian; (18–19) *Acanthohoplites bigoureti* (Seunes, 1887), UJF-ID.12240, Anzate section (AZ-11), *Acanthohoplites nolani* Zone, late Aptian; (20–21) *Protacanthoplites bogdanovae* (Tovbina, 1982), UJF-ID.12241, Anzate section (AZ-14), *Acanthohoplites nolani* Zone, late Aptian. All specimens x 1, except figures (15–16) x 1,5.

furcata Zone has not been formally characterized, because it lies within discontinuity D4 in most of the EAB sections (see section 6.1.). In Addar, the base of the zone is now placed within the discontinuity D4, according to the regional framework. The zone is characterized by a long list of representative Albian taxa (Table 1), including *Phyllopachyceras* aff. *baborense* (Plate 2.26–2.28), *Puzosia quenstedti* (Plate 2.36–2.37), *Parabrancoceras* sp. (Plate 2.17), *Oxytropidoceras* sp., *Parengonoceras* cf. *bassei, "Beudanticeras" revoili* (Plate 2.29–2.30), *Neosilesites palmensis* (Plate 2.31–2.32), *Hypacanthoplites* cf. *paucicostatus* (Plate 2.6–2.7), *Douvilleiceras leightonense, Mellegueiceras* cf. *jaillardi* (Plate 3.1–3.2), *Eogaudryceras* (*Eotetragonites*) cf. *gardneri*, *Tetragonites rectangularis*. In both the Ida w Shayq and Tinfoul sections, the base of the *L. tardefurcata* Zone is identified below the discontinuity D4, thanks to the presence of *Parasilesites kilianiformis* (Plate 2.33–2.35) and several species listed above.

5.1.10. Douvilleiceras mammillatum ammonite Zone

The zone is only formally documented in both the Tiskatine and Addar sections. *D. leightonense* (Plate 2.11–2.12) is considered a marker of the *L. tardefurcata* Zone. We place, therefore, the base of the *D. mammillatum* Zone at the occurrence of a doubtful "*Beudanticeras*" cf. *africana*, although the first strong criterion for the characterization is the occurrence of *D. mammillatum* (Plate 2.13–2.14). In Addar (Peybernes et al. 2013), the base of the zone is confirmed with the FO of *Parengonoceras hachourii* (Plate 2.15–2.16).

5.2. Calcareous nannofossil biostratigraphy

The preservation of calcareous nannofossils in the different sections of the EAB is poor to good. Uppermost Barremian to lower Aptian deposits are characterized by many sedimentary discontinuities corresponding to erosive surfaces; D0 and D1, for instance, correspond to karsted surfaces. All samples collected from the base of Ida w Shayq, Tiskatine and Addar successions were barren or yielded very rare and poorly-preserved nannofossils, which does not allow nannofossil zones to be characterized. However, the calcareous nannofossil zones NC6 to NC8 have been recognized in the EAB. Calcareous nannofossil markers are illustrated in Plate 4.

5.2.1. Chiastozygus litterarius Zone (NC6)

The NC6 Zone was defined as the interval between the FO of *H. irregularis* and the FO of *Eprolithus floralis*. It was subdivided into the NC6A (lower) and NC6B (upper) subzones, defined as the interval between the FO of *H. irregularis* and the LO of *Conusphaera rothii*, and as the interval between the LO of *C. rothii* and the FO of *E. floralis*, respectively (Bralower et al. 1993, 1995). The Zone NC6 is recognized in Ida w Shayq, Tiskatine, Addar and Alma sections, but its base is poorly-constrained. In Ida w Shayq, both subzones are recognized, whereas in other sections *Conusphaera rothii* is not recognized, not allowing to differentiate the two subzones. It is important to notice that in Ida, Tiskatine and Addar sections, the FO of *F. oblongus* postdates the FO of *H. irregularis* (Fig. 7).

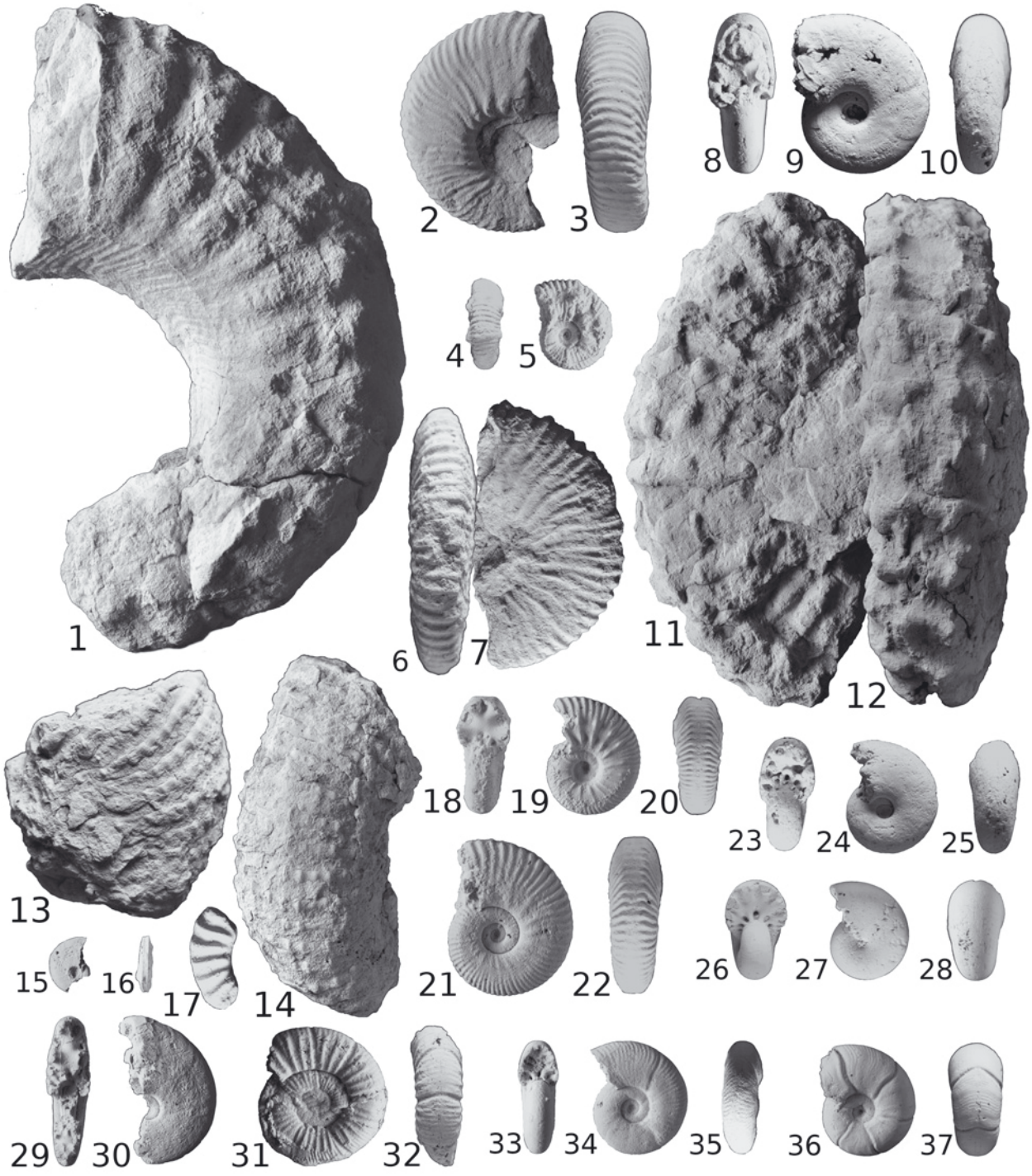
1
2
3
4
5
6
7
8
9
10
11
12
13
14
15
16
17
18
19
20
21
22
23
24
25
26
27
28
29
30
31
32
33
34
35
36
37

Plate 2. (1) *Pseudoaustraliceras hirtzi* (Collignon, 1962), UJF-ID.12242, Addar section (ADR-3), *Epicheloniceras martini* Zone, late Aptian; (2–3) *Elsaisabellia tiskatinensis* Luber et al. (2017), UJF-ID.12243, Tiskatine section (TKC-53), *Acanthohoplites nolani* Zone, late Aptian; (4–5) *Diadochoceras caucasicus* (Luppov, 1958), UJF-ID.12244, Anzate section (AZ-18), *Hypacanthoplites jacobi* Zone, late Aptian; (6–7) *Hypacanthopites* cf. *paucicostatus* (Breistroffer *in* Dubourdieu, 1953), UJF-ID.12245, Tiskatine section (TKC-65), *Hypacanthoplites jacobi* Zone, late Aptian; (8–10) *Pseudorbulites convergens* (Jacob, 1907), UJF-ID.12246, Addar section (ADR-22), *Leymeriella tardefurcata* Zone, early Albian; (11–12) *Douvilleiceras leightonense* Casey (1962), UJF-ID.12247, Tiskatine section (TKC-87), *Leymeriella tardefurcata* Zone, early Albian; (13) *Douvilleiceras mammillatum* (Schlotheim, 1813), UJF-ID.12248, Aoulkjdad section (TKE-36), *Douvilleiceras mammillatum* Zone, early Albian; (14) *Douvilleiceras mammillatum* (Schlotheim, 1813), UJF-ID.12249, Aoulkjdad section (TKE-36), *Douvilleiceras mammillatum* Zone, early Albian; (15–16) *Parengonoceras hachourii* (Breistroffer *in* Dubourdieu, 1953), UJF-ID.12250, Addar section (ADR-25), *Leymeriella tardefurcata* Zone, early Albian; (17) *Parabrancoceras* sp., UJF-ID.12251, Ida w Shayq section (IDA-29), *Leymeriella tardefurcata* Zone, early Albian; (18–20) *Hypacanthoplites clavatus* (Fritel, 1906), UJF-ID.12252, Ida w Shayq section (IDA-23), *Hypacanthoplites jacobi*, late Aptian, to *Leymeriella tardefurcata* Zone, early Albian; (21–22) *Hypacanthoplites elegans* (Fritel, 1906), UJF-ID.12253, Ida w Shayq section (IDA-22), *Hypacanthoplites jacobi*, late Aptian, to *Leymeriella tardefurcata* Zone, early Albian; (23–25) *Fallotermiericeras problematica* (Fallot & Termier, 1923), UJF-ID.12254, Addar section (ADR-17), *Leymeriella tardefurcata* Zone, early Albian; (26–28) *Phyllopachyceras baborense* (Coquand, 1880), UJF-ID.12255, Addar section (ADR-22), *Leymeriella tardefurcata* Zone, early Albian; (29–30) *"Beudanticeras" revoili* (Pervinquière, 1907), UJF-ID.12256, Tiskatine section (TKC-82), *Leymeriella tardefurcata* Zone, early Albian; (31–32) *Neosilesites palmensis* (Fallot & Termier, 1923), UJF-ID.12257, Alma section (AL-20), *Leymeriella tardefurcata* Zone, early Albian; (33–35) *Parasilesites kilianiformis* (Fallot, 1910), UJF-ID.12258, Ida w Shayq section (IDA-23), *Leymeriella tardefurcata* Zone, early Albian; (36–37) *Puzosia quenstedti* (Parona & Bonarelli, 1897), UJF-ID.12259, Anzate section (AZ-21), *Leymeriella tardefurcata* Zone, early Albian. All specimens x 1.

5.2.2. Rhagodiscus angustus Zone (NC7)

The NC7 Zone was defined as the interval between the FO of *E. floralis* and the FO of *Prediscosphaera columnata*. It is recognized in all sections and spans from the *E. martini* to *L. tardefurcata* ammonite zones (Figs 7–8). *Micrantholithus hoschulzii* is found sporadically in the lower part of the late Aptian, in both Ida w Shayq and Addar sections; its LO lies in the *E. martini* Zone. Sporadic occurrences of *Rhagodiscus achlyostaurion* are observed from the early Aptian in Ida w Shayq (Fig. 7), but its first consistent occurrence (FCO is used after a species is recorded in consecutive samples (Ferreira et al. 2019)), is generally observed from the upper part of the late Aptian, in the upper part of the NC7 Zone, (*A. nolani* to *H. jacobi* ammonite zones; Figs. 7–8). Several nannofossil taxa first occur in the lower part of the late Aptian: *Orastrum perspicuum, Braarudosphaera* spp. (*B. africana* and *B. hockwoldensis*), *Diloma californica, Eiffelithus hancockii.* These FOs are all recognized in Ida w Shayq, Tiskatine and Addar sections and generally lie in the *E. martini* Zone (Fig. 7). The nannoconid association, composed of specimens with a wide central cavity, such as *N. circularis*, *N. wassallii*, and *N. vocontiensis* last occurs in the lower part of the late Aptian (Fig. 7). The LO of *D. californica* is also recognized in the upper part of the NC7 Zone and lies in the *A. nolani* to *H. jacobi* ammonite zones, depending on the sections (Figs. 7–8). The LO of *M. obtusus* and *Zebrashapka vanhintei* are also recognized in the upper part of the late Aptian, but not recorded in all sections, probably due to sporadic occurrence of these species throughout the different successions (Figs. 7–8).

5.2.3. Prediscosphaera columnata Zone (NC8)

The NC8 Zone was defined as the interval between the FO of *Prediscosphaera columnata* and the FO of *Axopodorhabdus albianus* and subdivided into three subzones, called respectively A, B and C (Bralower et al. 1993, 1995). The NC8A Subzone was represented as the interval between the FO of *P. columnata* and the FO of *Hayesites albiensis*. The NC8B Subzone was defined as the interval between the FO of *H. albiensis* and the FO of *Tranolithus orionatus*, and the NC8C Subzone was represented as the interval between the FO of *T. orionatus* and the FO of *A. albianus*. Because the FO of *T. orionatus* was not recognized in the studied sections, only the NC8A and the lower part of the NC8B have been identified in the EAB. Elliptical *P. spinosa* and subcircular to circular *P. columnata*, ranging in size from 3 to 5 µm, were encountered in the EAB (Figs 7–8). The base of the NC8 Zone, defined by circular forms, lies in the latest Aptian

Plate 3. (1–2) *Mellegueiceras jaillardi* Latil (2011), UJF-ID.12260, Tiskatine section (TKC-79), *Leymeriella tardefurcata* Zone, early Albian, x 1.

(*H. jacobi* Zone) in both Ida w shayq and Tinfoul, where the Aptian–Albian boundary is placed immediately below D4. In other sections, the base of the NC8 lies in the earliest Albian, where the base of the *L. tardefurcata* Zone is placed within D4 (Figs 7–8). *H. albiensis* was defined by Perch-Nielsen (1985) as an early Albian species showing a star shape with 6–8 long rays. Bown (in Kennedy et al. 2000) identified a transitional form between *H. irregularis* and *H. albiensis* with regular 5–7 short radially arranged rays, that he called *Hayesites* cf. *H. albiensis* (Bown 2005). This form is recognized in Ida w Shayq, Addar, Tiskatine and Alma sections, and its FO is recorded just above D4, in the early Albian *L. tardefurcata* Zone (Figs. 7–8). The totality of the NC8A Subzone is recognized in Addar, Tiskatine and Anzate. Other FOs are recognized in this Subzone, including the FO of *Arkhangelskiella stenostaurion* in Addar, Anzate, Alma and Tinfoul, and the FO of *Helicolithus trabeculatus* in Addar and Anzate, both in the *L. tardefurcata* Zone (Figs. 7–8).

5.3. Carbon isotope record

In the Ida w Shayq section, the $\delta^{13}C_{carb}$ values vary between –1.2 and 0.9‰ (Fig. 9). Although fluctuating, they generally increase in the Aptian succession, with positive values up to 0.9‰ above D2 in the late

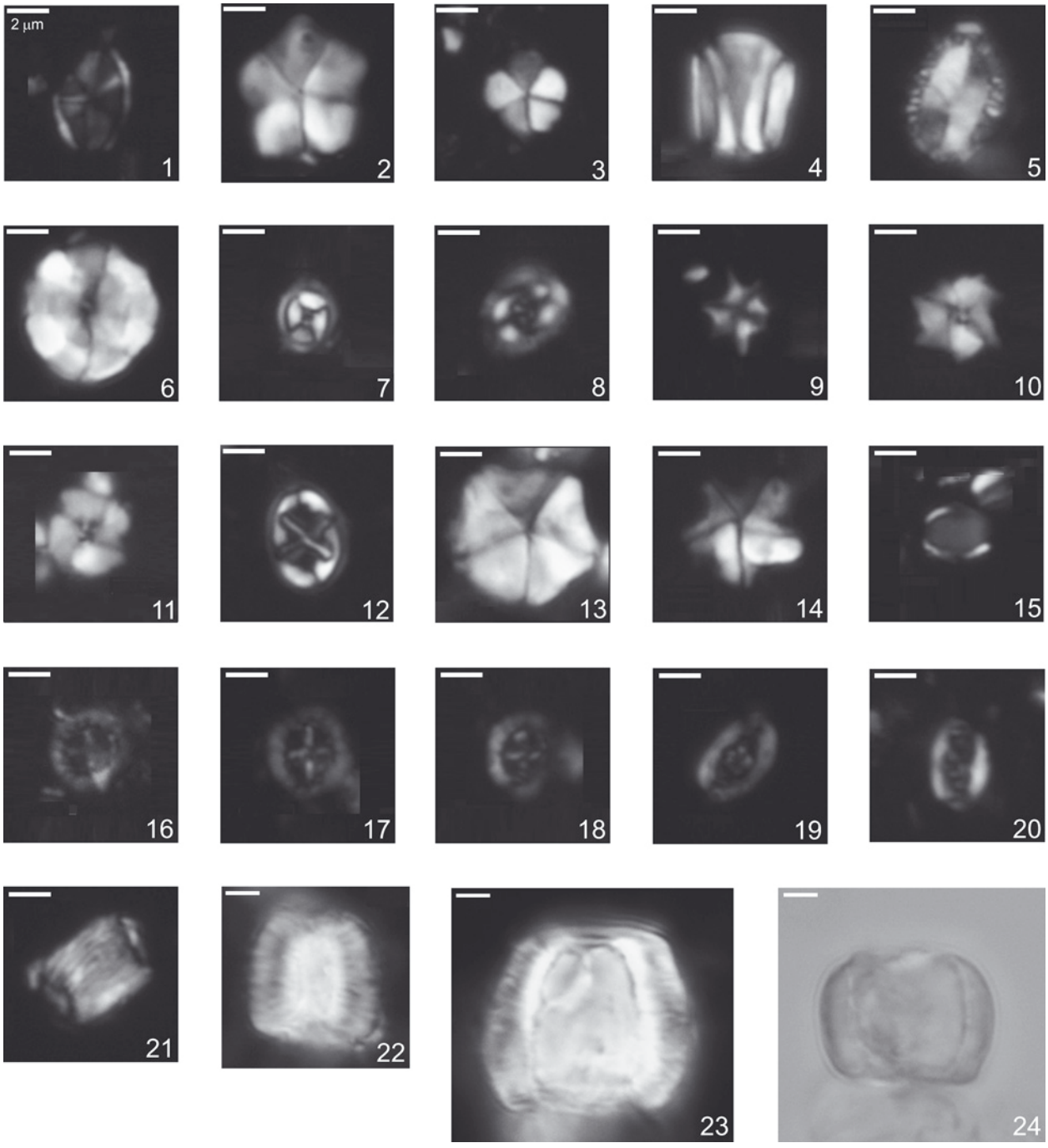

Plate 4. Photomicrographs of selected nannofossil species from the Essaouira-Agadir Basin. 1, *Arkhangelskiella stenostaurion*, XLP, sample AddN28. 2, *Braarudosphaera africana*, XLP, sample AddN41. 3, *Braarudosphaera hockwoldensis*, XLP, sample AddN11. 4, *Conusphaera rothii*, XLP, sample Idm9. 5, *Diloma californica*, XLP, sample AddN11. 6, *Eprolithus floralis*, XLP, sample Anz1. 7, *Eiffelithus hancockii*, XLP, sample Tf2. 8, *Flabellites oblongus*, XLP, sample Anz4. 9, *Hayesites albiensis*, XLP, sample TC113. 10, *Hayesites* cf. *H. albiensis*, XLP, sample Anz4. 11, *Hayesites irregularis*, XLP, sample Idm11. 12, *Helicolithus trabeculatus*, XLP, sample Anz4. 13, *Micrantholithus hoschulzii*, XLP, sample AddN6. 14, *Micrantholithus obtusus*, XLP, sample Idm4. 15, *Orastrum perspicuum*, XLP, sample AddN6. 16, *Prediscosphaera columnata*, circular form, XLP, sample Anz47. 17, *Prediscosphaera columnata*, subcircular form, XLP, Alma23. 18, *Prediscosphaera spinosa*, XLP, sample Tf2. 19, *Rhagodiscus achlyostaurion*, XLP, sample AddN30. 20, *Rhagodiscus gallagheri*, XLP, sample Tf16. 21, *Zebrashapka vanhintei*, sample AddN13. 22, *Nannoconus truittii truittii*, XLP, sample Tf11. 23, *Nannoconus vocontiensis*, XLP, sample Idm9. 24, *Nannoconus circularis*, TL, sample Idm7. Scale white bar: 2 microns for all photomicrographs.

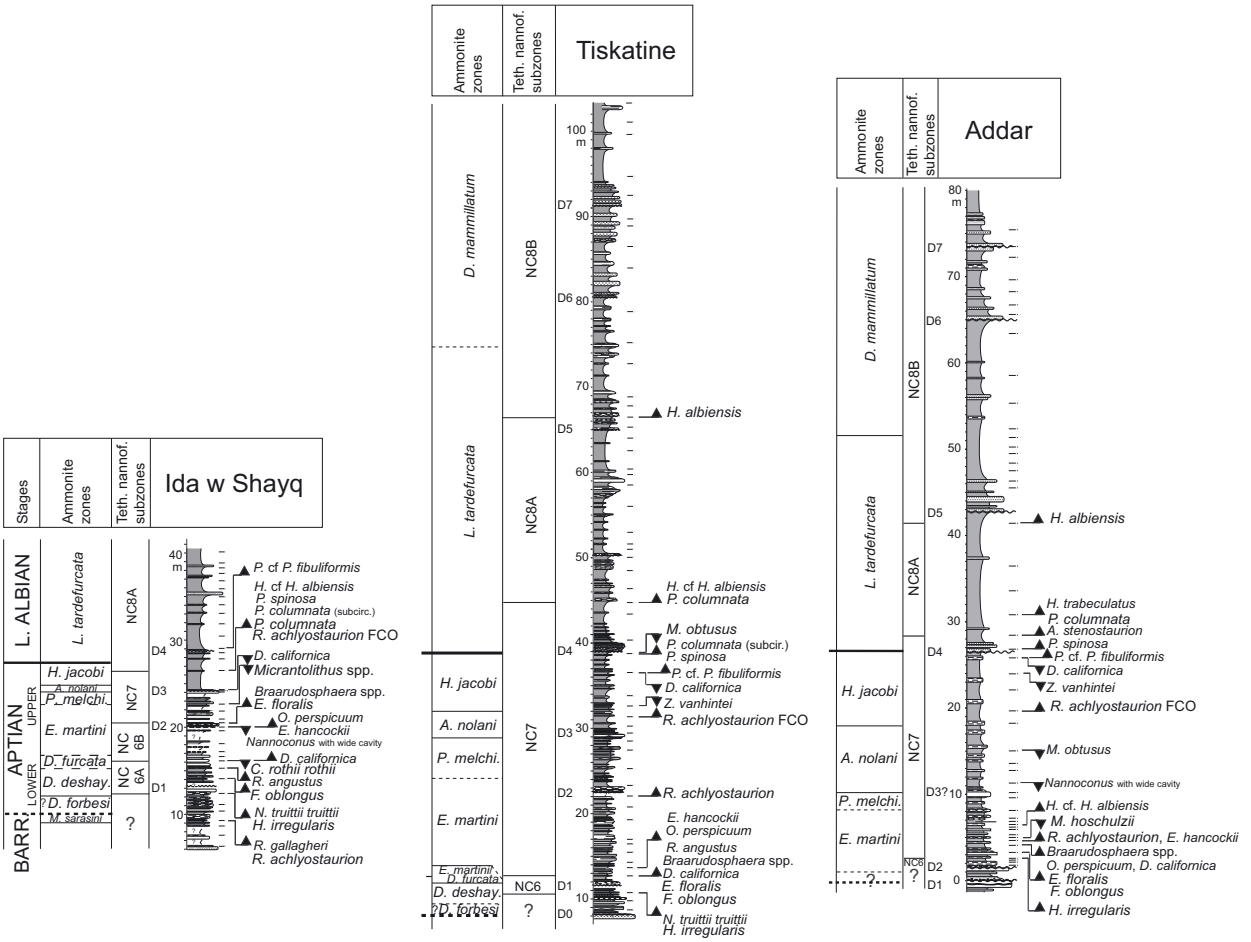

Fig. 7. Calcareous nannofossil bioevents recorded in the latest Barremian–early Albian of Ida w Shayq, Tiskatine and Addar sections, plotted against the ammonite zonation. Abbreviations: D, sedimentary discontinuities; FCO, first consistent occurrence.

Aptian. From the latest Aptian to the early Albian, the $\delta^{13}C_{carb}$ values decrease slowly, achieving the most negative values around D4. From D4 to the top of the succession, only small variations are observed. In the Tiskatine section, the $\delta^{13}C_{carb}$ values vary between –1.6 and 1.8‰ (Fig. 9). They increase in Aptian times, reaching a maximum before D4. Then, they decrease upward reaching a minimum above D6, before increasing again in the upper part of the succession. In the Addar section, the $\delta^{13}C_{carb}$ values vary between –7.6 and 1.4‰ (Fig. 9). After a slight increase at the base of the section, they show a plateau in the late Aptian. Then, $\delta^{13}C_{carb}$ decrease to a minimum of –7.6‰ just above D4. In the early Albian, the $\delta^{13}C_{carb}$ values stay negative with two very short decrease and increase around meters 51 and 68.5, respectively. In the Alma section, the $\delta^{13}C_{carb}$ values vary between –3.8 and 1.5‰ (Fig. 9). Lowest values are remarkable in the lowermost part of the succession and increase in the early Aptian, reaching a plateau in the early late Aptian, and then increase to reach a maximum just above D3. After a slight decrease in the latest Aptian, $\delta^{13}C_{carb}$ slightly increase until the Aptian–Albian boundary, below D4. They slightly decrease in the early Albian. In the Anzate section, the $\delta^{13}C_{carb}$ values ranges from –4.6 to 0.2‰ and decrease from the base of the succession (late Aptian) till discontinuity D5 (Fig. 9). Above D5, they increase and reach a maximum at 73 meters. Then, values firstly decrease then increase in the uppermost part of the studied interval. In the Tinfoul section, the $\delta^{13}C_{carb}$ values vary between –3.3 and 0.9‰ (Fig. 9). After a slight increase recorded in the late Aptian, they decrease reaching –2‰ just above D5, and then slightly increase to form a plateau in the middle part of the *D. mammillatum* Ammonite Zone. Above, values reach a minimum and then increase at the top of the section.

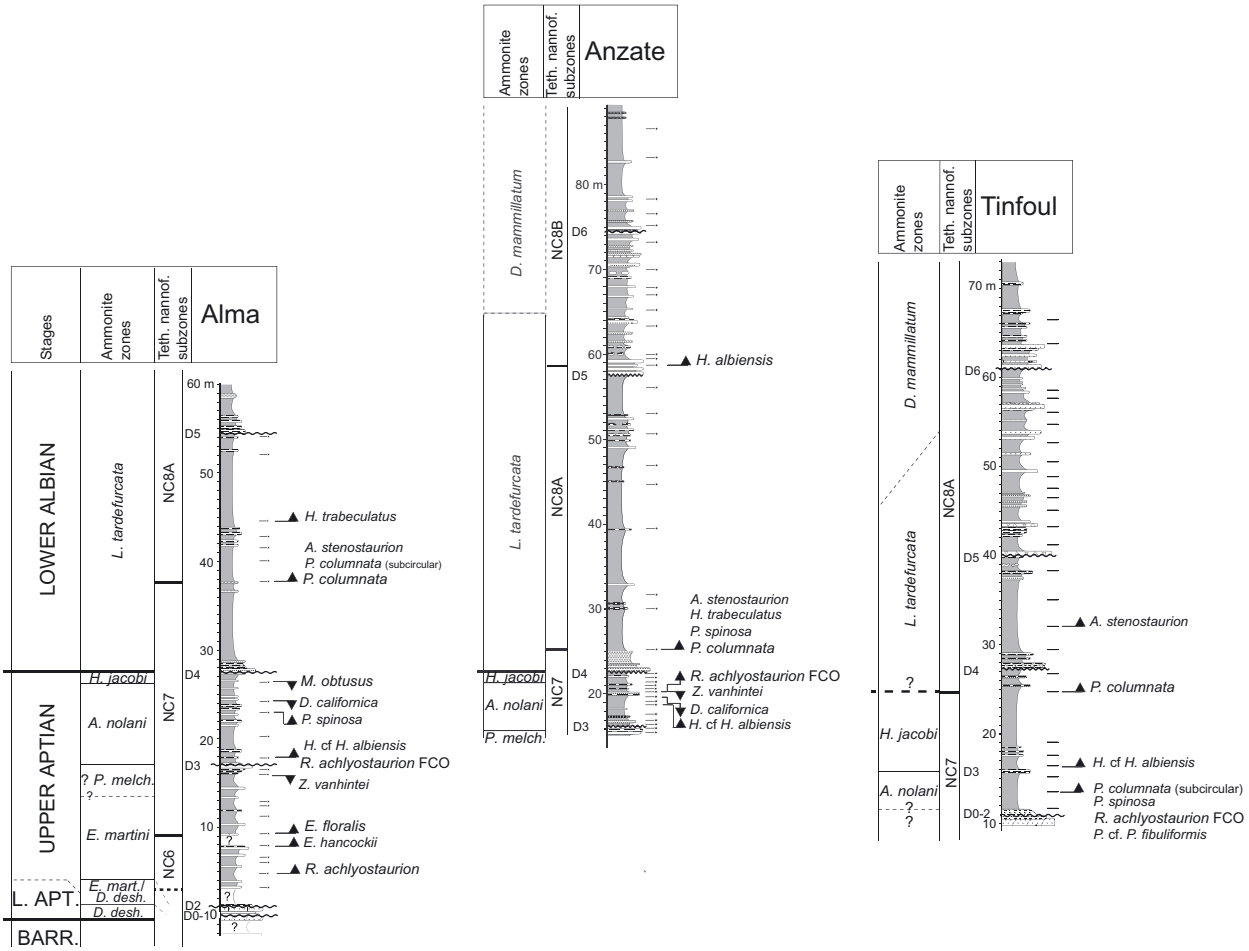

Fig. 8. Calcareous nannofossil bioenvents recorded in the latest Barremian–early Albian of Alma, Anzate and Tinfoul sections, plotted against the ammonite zonation. Abbreviations: D, sedimentary discontinuities; FCO, first consistent occurrence.

6. Discussion

6.1. Ammonite biostratigraphy

The distribution of ammonite populations of the EAB has been calibrated with the Standard Mediterranean Zonation proposed by the IUGS Lower Cretaceous Ammonite Working Group (Reboulet et al. 2018; Fig. 10). The zones are assemblage or interval zones. Their bases are defined either by the FO of the index species when present, or the FO of other representative taxa. Accurate location of the zone boundaries on each section has proven difficult. Repeated hiatuses and condensed levels have been recognized in the whole succession: superimposed discontinuities at the base of the Anzate and Alma sections, discontinuity D3 encompassing an undefined part of the lower *A. nolani* Zone and the upper (? major) part of the *P. melchioris* Zone in Ida w Shayq, among other examples. The bases of the Aptian and Albian stages may be positioned in sedimentary discontinuities. The base of the *Leymeriella tardefurcata* Zone coincides with discontinuity D4 in a large part of the basin (Fig. 10), except in Ida w Shayq and maybe in Tinfoul, where it is identified immediately below D4.

Our interpretation differs from that proposed by Luber et al. (2017), especially regarding the assumption of a long-lasting early Aptian to lowermost late Aptian hiatus. It must be first noticed that figures of Luber et al. (2019) partly contradict their assumption proposed in 2017. In Luber et al. (2019), the ammonite associations and calibration of *D. forbesi* and *D. furcata* zones in the text-figure 4 (Id Amran section) is in contradiction with the text-figure 7 (see hiatus of the *D. furcata* Zone) and with the conclusion assumed in Luber et al. (2017). But,

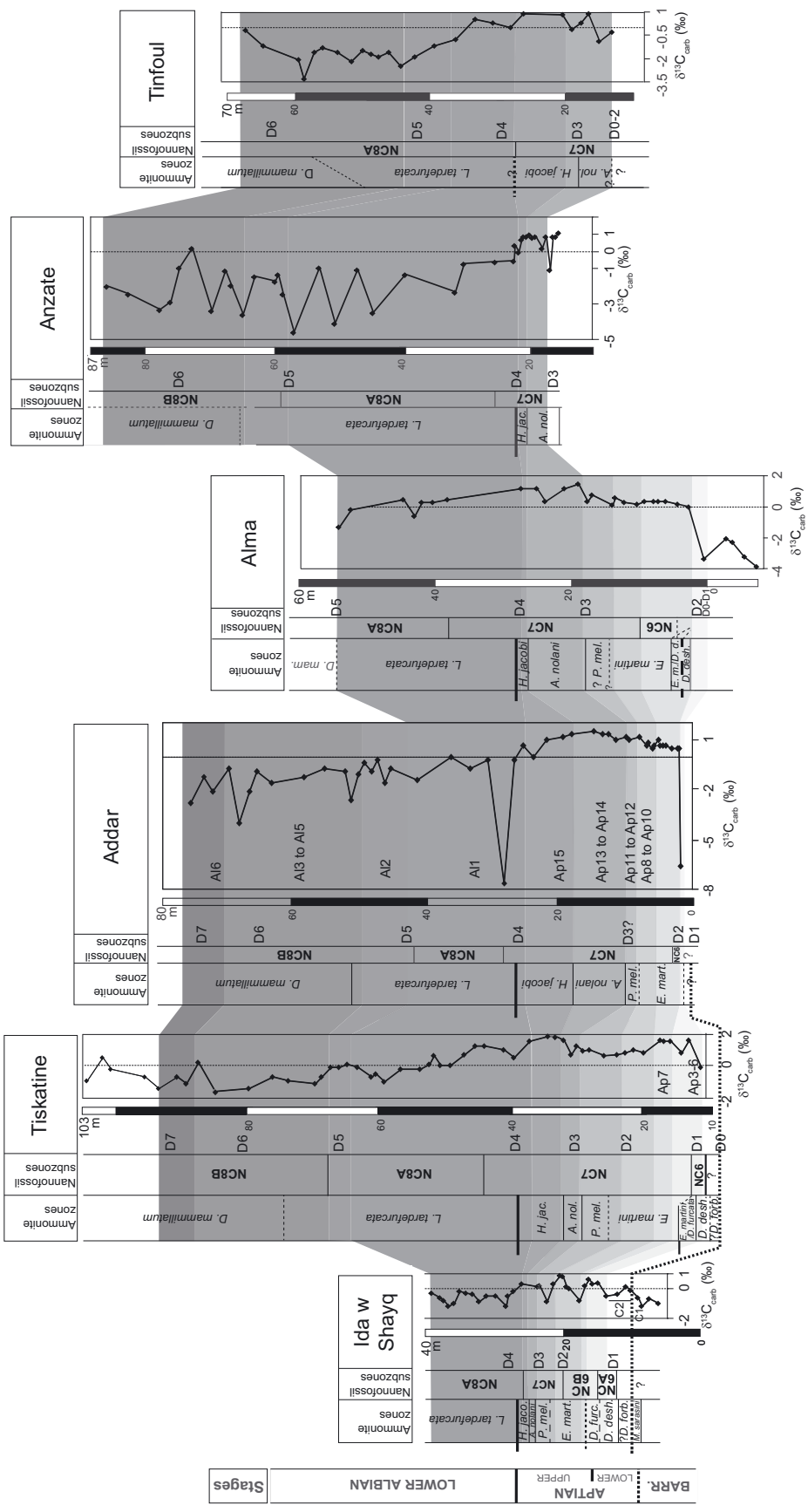

Fig. 9. Carbon isotope records for the latest Barremian–early Albian of the six studied sections in the EAB, plotted against biostratigraphy. Correlations between the sections are based on the recognition of carbon isotope segments/units previously defined by Menegatti et al. (1998) and Herrle et al. (2004).

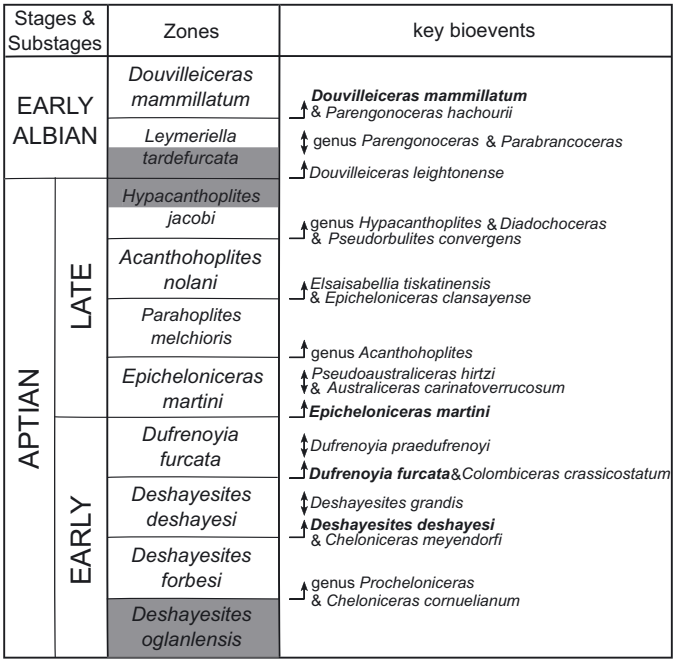

Fig. 10. Biostratigraphic chart: Tethyan ammonite nomenclature ("Kilian Group", Reboulet et al. 2018) and major key bioevents of the EAB. Hiatuses are in grey.

above all, we found index-species and representative taxa of the *D. deshayesi*, *D. furcata* and of the base of the *E. martini* zones (Fig. 10).

The latest Barremian *Martelites sarasini* Zone is recorded for the first time in the EAB, in the Ida w Shayq section, with occurrence of *Kutatissites* sp. and *Pseudocrioceras* sp. Because of discontinuity surfaces and related sedimentary hiatuses, the *Deshayesites oglanlensis* Zone is not identified (Fig. 10). In Ida w Shayq and Tiskatine, the *D. forbesi* Zone is tentatively recognized with the first Cheloniceratids associations (Delanoy 1997, Ropolo et al. 2006, Moreno Bedmar et al. 2009). This calibration is supported by data from other sections of the EAB, such as Takoucht and Aoulkjdad (not presented here). It is consistent with the proposition of Luber et al. (2017) of a *Procheloniceras dechauxi* Zone as equivalent *pro parte* of the lower part of the *D. forbesi* Zone. The subsequent three ammonite zones are attested by the presence of the index-species (Fig. 10), and several other Tethyan species, listed in section 5.1 (see Casey 1998, Dutour 2005, Moreno Bedmar et al. 2009, 2010).

We place the base of the *Acanthohoplites nolani* Zone at the base of the "Nolani Beds", while isolated specimens of the genus *Elsaisabellia* are pointed few meters below. The latter genus, associated with numerous Acanthohoplitids, largely dominates the very rich assemblage of the zone (see Casey 1965a, b, Robert et al. 2001, Dutour 2005, Bulot et al. 2014). This interpretation is in line with the proposition of Luber et al. (2017).

As shown by Peybernes et al. (2013) and Luber et al. (2017), the FO of *Hypacanthoplites* is systematically located above the *Elsaisabellia* levels. We consider that the *Hypacanthoplites* distribution begins at the base of the *H. jacobi* Zone (Robert et al. 2001), together with *Pseudorbulites convergens*. The upper part of the *H. jacobi* Zone is considered as generally comprised within the discontinuity D4 (Fig. 10). In our record, the genus *Diadochoceras* also appears few meters above the *Elsaisabellia* levels, in contrast with Luber et al. (2017), who found both genera associated. In the EAB, the genus *Diadochoceras* first appears in the upper part of the *A. nolani* Zone, whereas a *D. nodosocostatum* Subzone was designed as the lower part of the *A. nolani* Zone in other Mediterranean settings (Reboulet et al. 2018).

The use of *Mellegueiceras chihaouiae* as index of an early Albian zone by Luber et al. (2017) is erroneous. As matter of fact, according to Latil (2011) and Ben Chaabane et al. (2019), *M. chihaouiae* cannot be restricted to the early Albian but rather characterizes the Aptian-Albian transition. Although its base is not formally identified, the *L. tardefurcata* Zone is better evidenced by the occurrence of several *Douvilleiceras leightonense* and *Douvilleiceras* sp., associated with other first-rate markers, such as *Oxytropidoceras* sp., *Parengonoceras bassei* and/or *Parabrancoceras* sp.

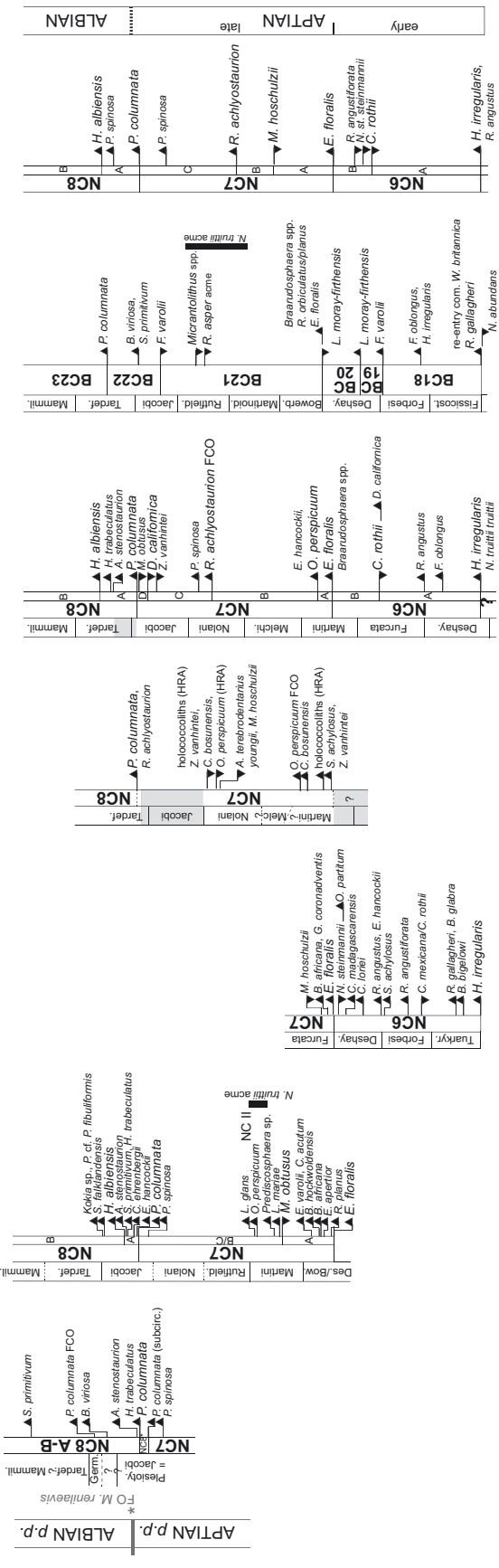

Fig. 11. Calcareous nannofossil zonation defined for the EAB and its comparison with existing biozonation schemes where both ammonite and nannofossil records were calibrated. See the text for more explanation.

Calibration may also be supported by the presence of the genus *"Beudanticeras"* (Bréhéret et al. 1986, Kennedy 2004, Kennedy et al. 2000, Latil 2011), or by the species *Hypacanthoplites paucicostatus* (Robert et al. 2001), *Mellegueiceras jaillardi* (Latil 2011), *Eogaudryceras* (*Eotetragonites*) *gardneri* and *Tetragonites rectangularis* (Murphy 1967).

6.2. Aptian-early Albian nannofossil biostratigraphy

Twenty-four calcareous nannofossil bioevents have been recognized in this work (Figs. 7–8). Among them, 19 most reliable bioevents are summarized in Figure 11; 4 of which correspond to new bioevents. The NC7 subzones defined by Bralower et al. (1993) are emended here and a new subzone is introduced. Both emended and new subzones are established through easily recognizable index species (Plate 4), or species occurring amidst different successions. Nannofossil bioevents are plotted against synthetic ammonite biozonation recognized for the EAB (Fig. 11).

6.2.1. NC7A Subzone

Defined by Bralower et al. (1993), the NC7A Subzone is emended herein. Bralower et al. (1993) chosed to define the top of this subzone by the LO of *Micrantholithus* spp. However, the LO of the latter is difficult to determine (Erba et al. 1999, Moullade et al. 2015, Giraud et al. 2018), and is thus of problematic use as a subzonal marker. The top of this Subzone is thus emended, and is defined by the FO of *Orastrum perspicuum*. The FO synchronicity of *O. perspicuum* (within *E. martini* Zone) in Ida w Shayq, Tiskatine and Addar sections renders this species a robust and easily identifiable marker for the base of the late Aptian. The FO of *O. perspicuum*, also recognized in the Tiskatine section of Luber et al. (2019) and in the Vocontian Basin (SE France; Herrle and Mutterlose 2003), represents a reproducible bioevent for the basal late Aptian (Fig. 11). This bioevent needs to be better investigated in other basins.

6.2.2. NC7B Subzone

Defined by Bralower et al. (1993) and emended herein, this subzone ranges from the FO of *O. perspicuum* to the first consistent occurrence (FCO) of *Rhagodiscus achlyostaurion*. It spans throughout part of the late Aptian, from the basal *E. martini* Zone up to the *A. nolani* Zone. Bergen (1998) mentioned that "there is a wide disagreement over the age of the FO of *R. achlyostaurion*", used to define the top of the NC7B Subzone by Bralower et al. (1993). Depending on settings, its FO was recorded from the late Barremian to the early Albian (Erba 1988, Bralower et al. 1993, Bergen 1994, de Kaenel & Bergen 1996, Bown 2005). The FCO synchronicity of *R. achlyostaurion* (within *A. nolani* Zone) in four sections of the EAB (Tiskatine, Alma, Anzate, Tinfoul) shows that it is a more robust bioevent compared to its FO, and it is, therefore, chosen to define the top of the NC7B Subzone. The FO of *Eiffelithus hancockii*, which also seems to be a reproducible bioevent within the EAB, characterizes the base of this subzone.

6.2.3. NC7C Subzone

Defined by Bralower et al. (1993) and emended herein, this subzone ranges from the FCO of *R. achlyostaurion* to the LO of *Diloma californica*. It spans the upper part of the late Aptian, from the *A. nolani* Zone up to the *H. jacobi* Zone. The LO of *D. californica* can be used to better constrain the upper part of the late Aptian. Both the FO and LO of this species, which has only been reported in the Aptian of northern California (USA, Fernando and Okada 2007), were previously not constrained. The stratigraphic range of *D. californica* is defined in the present study as latest early Aptian (*D. furcata* Zone) up to the upper part of the late Aptian (*H. jacobi* Zone). Further investigations of both the FO and LO of this easily recognizable species in other basins will be necessary to check whether these bioevents are reproducible. The reference section for the NC7C Subzone is Tiskatine. Within this subzone is observed the LO of *Zebrashapka vanhintei*.

6.2.4. NC7D Subzone

Defined herein, this subzone ranges from the LO of *D. californica* to the FO of *Prediscosphaera columnata* (circular form). It spans across the latest Aptian, within the upper part of the *H. jacobi* Zone. The LO of *Micrantholithus obtusus* occurs within this subzone.

The biostratigraphic frame established in the present study, based on both nannofossils and ammonites is more accurate and inclusive with respect to that defined by Luber et al. (2019; Fig. 11). The latter authors proposed their Tiskatine section as a type section for the Aptian of NW Africa, whereas only

part of the late Aptian (from *E. martini* to *A. nolani* ammonite zones and part of the NC7 Zone) is represented there (Fig. 11). The Tiskatine section selected by Luber et al. (2019) corresponds to the Taounerine section described in Jaillard et al. (2019a); in the latter section, the Aptian–Albian time interval is less well-recorded than in the Tiskatine section of the present study.

6.3. Comparison of the Aptian–early Albian nannofossil biostratigraphic scheme of the EAB with other basins

The succession of nannofossil bioevents observed in the EAB presents some discrepancies when compared with those of other basins; possible causes for such inconsistencies are discussed here. In Fig. 11, we have reported only studies that calibrated nannofossil bioevents with ammonite zonation; the Aptian–early Albian Tethyan nannofossil zones defined by Bralower et al. (1993), and biostratigraphic markers used to define the GSSP for the base of the Albian stage in the Pré-Guittard section, have also been reported.

The FO of *Rhagodiscus gallagheri* lies in the latest Barremian (*M. sarasini* ammonite Zone) in the EAB. In other Tethyan basins, the age of its FO varies from the late Barremian (Aguado et al. 1997, 1999) up to the early Aptian (Giraud et al. 2018; Fig. 11). This apparent diachronism in the FO of *R. gallagheri* may be related to different taxonomic concepts used in its identification, since it is a problematic taxon. This small narrowly elliptical *Rhagodiscus* species has been previously included within the species concept of *R. angustus* (Thomsen 1987, Mutterlose 1991); specimens are transitional in outline between *R. angustus* and *R. asper* (Bergen 1998).

Both *Hayesites irregularis,* zonal marker of the NC6, and *Flabellites oblongus* are first recorded within the early Aptian (*D. deshayesi* ammonite Zone) in the EAB, as also recognized in boreal basins (Bown et al. 1998), whereas they have earlier FOs in other Tethyan sections (Fig. 11). The younger age of the base of the NC6 Zone recorded in the EAB with respect to other Tethyan sites is interpreted as due to both a very poor preservation (frequent dolomitization), and a hiatus, corresponding to the discontinuity D0 that encompasses the Barremian–Aptian boundary and earliest Aptian times.

In the EAB, the LO of *Conusphaera rothii*, subzonal marker of the NC6B, is recorded later in the early Aptian (*D. furcata* ammonite Zone) than reported in the Cassis-la-Bédoule section (SE France, Bergen 1998; Fig. 11). The LO of *C. rothii* is generally difficult to establish in land sections due to poorer preservation and rarity of this taxon, with respect to deep-sea sections (Bralower et al. 1993). The present study thus allows to better constrain the LO of the zonal maker *C. rothii*.

The FO of *Eprolithus floralis*, zonal marker of the NC7, is recorded in the EAB in the lowermost part of the late Aptian (*E. martini* ammonite Zone), which is younger than its FO generally observed in the early Aptian of other areas (Aguado et al. 1999, Erba et al. 1999, Luciani et al. 2006, Moullade et al. 2015, Giraud et al. 2018, Szives et al. 2018), close to the *D. deshayesi/D. furcata* ammonite zones boundary (Fig. 11). Poorly-preserved early Aptian nannofossil assemblages observed in the EAB cannot explain the younger occurrence of *E. floralis* because this species is considered a resistant-dissolution taxon (Bralower 1988). The late Aptian occurrence of this bioevent in the EAB might be of regional and/or paleoenvironmental significance.

The LO of *Micrantholithus obtusus* is observed in the EAB as late as in the latest Aptian (*H. jacobi* ammonite Zone), which is younger than in other northern Tethyan/boreal basins (Fig. 11). However, the occurrence of *Micrantholithus* spp. is sporadic in the Aptian of the EAB, as also mentioned for other Tethyan sections. Both the sporadic occurrence of *Micrantholithus*, depending on settings, and the diachronism of its LO, suggest that this bioevent is not reliable for biochronological purposes.

The FO of *Prediscosphaera columnata* (circular form), zonal marker of the NC8, lies within the latest Aptian in the EAB (*H. jacobi* Zone) and in different Tethyan basins (Fig. 11). Therefore, the FO of *P. columnata* (circular form) represents a reproducible bioevent in the Tethyan realm, which is of prominent importance as it lies close to the Aptian–Albian boundary.

In the EAB, the FO of *Hayesites albiensis*, subzonal marker of the NC8B, lies in the earliest Albian, within the *L. tardefurcata* Zone, which is later than the same FO reported by Bralower et al. (1993), who used it as an uppermost Aptian subzonal marker, and by Herrle and Mutterlose (2003), who identified it in the latest Aptian (*H. jacobi* Zone) of the Vocontian Basin (Fig. 11). Different taxonomic concepts could then explain discrepancies reported in the FO of *H. albiensis*. Specimens figured in Herrle and Mutterlose (2003, Fig. 6 x–w) resemble the transition forms (*Hayesites* cf. *H. albiensis*) and not the typical *albiensis*, since

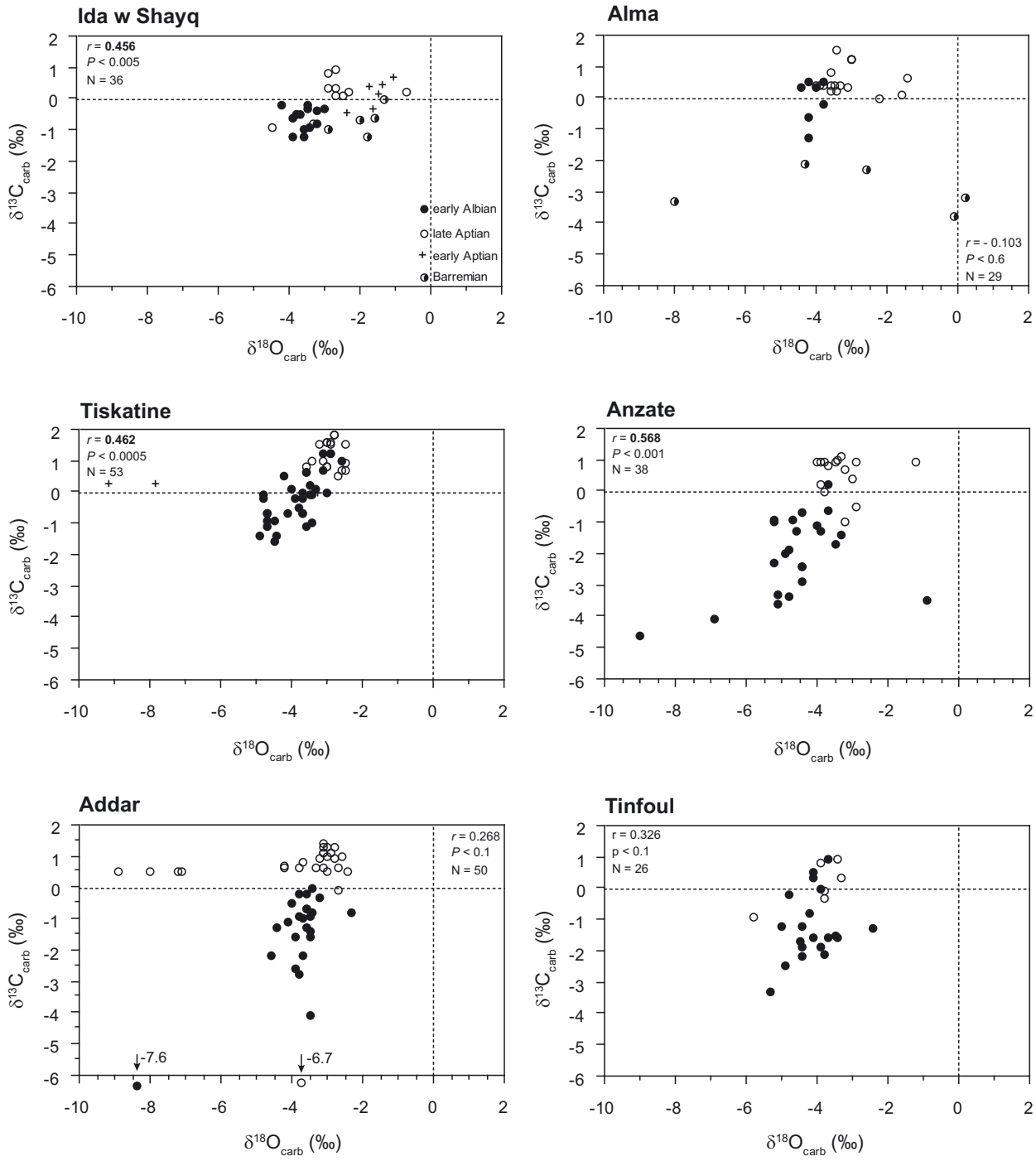

Fig. 12. Bivariate plot showing the relationship between $\delta^{18}O$ and $\delta^{13}C_{carb}$ values of whole rock for each of the six sections in the EAB. The correlation coefficient of Pearson *r* is in bold where it is statistically significant (*p* (probability) < 0.05) Abbreviations: N, number of measurements.

long free rays are not present. In the EAB, *Hayesites* cf. *H. albiensis* is recorded since the late Aptian, whereas typical *albiensis* with long free rays is observed from the early Albian onwards (Figs. 7–8, 11). As reported by Perch-Nielsen (1985), and then confirmed with the present study, *H. albiensis* with long free rays is a typical lower Albian form and is then useful for biostratigraphy.

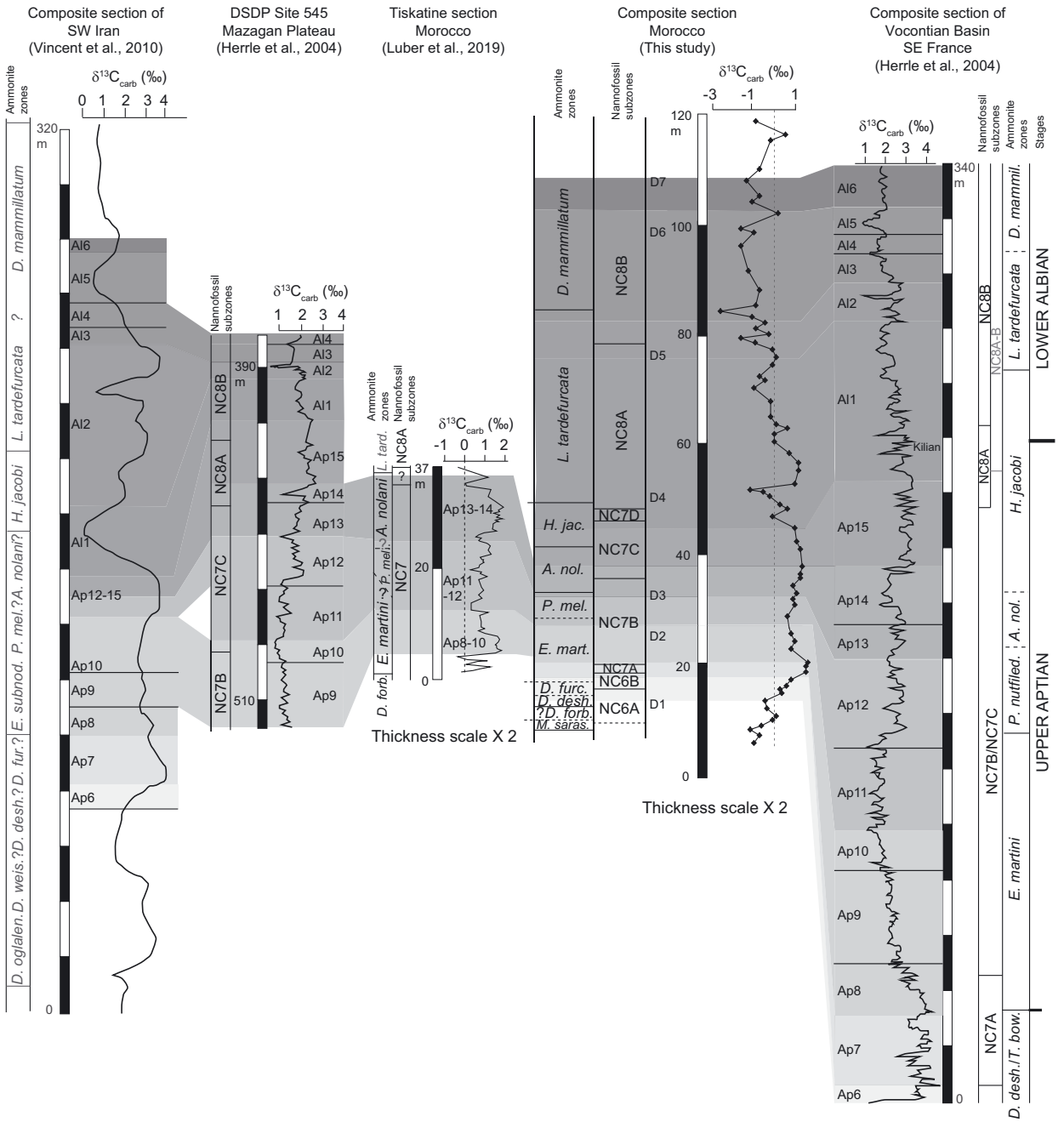

Fig. 13. Comparison of bio-and carbon isotope stratigraphies between the EAB and other settings for the latest Barremian–early Albian. The Aptian–Albian boundary is placed following Kennedy et al. (2017), with the boundary point lying just below the "Niveau Kilian" in the Vocontian Basin. The nannofossil zones in grey correspond to those recognized by Bown in Kennedy et al. (2017).

6.4. Carbon isotope record

The studied Moroccan sections belong to a marine mixed carbonate/siliciclastic ramp (see section 3). Shallow-marine carbonate successions generally present a complex geochemical record because sediments are commonly first exposed to meteoric water before reaching mineralogical stability (Allan and Matthews 1982). In a secondary stage, successions can also be exposed to burial diagenesis. Cement type can be diagnostic of a particular diagenetic environment. However, identical cement types may be formed in

different diagenetic environments. Equant drusy spar cement may precipitate in near-surface meteoric environments and under deep burial conditions (Flügel 2004). Most of the studied successions are made of fine-grained shale and marlstone with few limestone and sandstone interbeds. Cementation in the shale and marly beds is difficult to identify using transmitted light microscopy. In limestone and sandstone beds, the cementation showed a drusy mosaic spar cement filling intergranular pore spaces, and reaching about 20 % of the total rock components. This indicates cementation under influence of meteoric water for the uppermost Barremian–lower Albian sediments. Presence of coarse-crystalline dolomite rhombs, representing about 25 % of the total rock, reflects the occurrence of dolomitization processes after cementation during early late diagenetic stage, in the mixing zone with meteoric water. Because dolomitization has been well recognized very close to karsted surfaces influenced by meteoric water (see section 3), it most likely resulted from the change of the depositional suite during short-term relative global sea-level fall (El Araby 1999) or from karstification during a relative sea-level fall (Moss and Tucker 1996). However, these processes are limited to limestone and sandstone beds, which were little sampled for geochemistry. The $\delta^{13}C_{carb}$ and $\delta^{18}O_{carb}$ values of whole carbonate rocks can be altered by the occurrence of isotopically light meteoric cements and recristallized/neoformed carbonates during burial diagenesis. If analyzed sedimentary rocks were substantially affected by burial diagenesis, a strong positive correlation between oxygen and carbon-isotope values should have resulted (Jenkyns and Clayton 1986, Marshall 1992, Jenkyns 1996). Daoudi et al. (2010) showed with clay minerals analysis that, in the Agadir area of the EAB, the middle Albian interval was buried up to 1800 meters, indicating that this part was subjected to deep burial. Among the six studied successions, only three (Ida w Shayq, Tiskatine and Anzate) show a statistically significant positive correlation between $\delta^{18}O_{carb}$ and $\delta^{13}C_{carb}$ (r around 0.5; Fig. 12), suggesting that sedimentary $\delta^{13}C_{carb}$ values were little to moderate, generally not significantly affected by burial diagenesis in the EAB.

In the EAB, general trends in the $\delta^{13}C_{carb}$ values can be recognized and were used to establish a carbon isotope stratigraphy calibrated to both ammonite and calcareous nannofossil biostratigraphy (Fig. 9). The late Barremian is characterized by negative $\delta^{13}C_{carb}$ values, with an increase in the uppermost part. The early Aptian was bounded by a first minimum $\delta^{13}C_{carb}$ value at the base and a first maximum value at the early/late Aptian boundary. The late Aptian interval is characterized by gently increasing and positive $\delta^{13}C_{carb}$ values, but smaller fluctuations can also be detected. The Aptian/Albian boundary was recognized by a decrease of the $\delta^{13}C_{carb}$ values. Early Albian times (*L. tardefurcata* to lowermost part of the *D. mammilatum* zones, NC8A to lowermost part of the NC8B zones) were represented by a large decrease of more than 3‰ with minimum $\delta^{13}C_{carb}$ values, just interrupted by a slight increase in the upper part of the *L. tardefurcata* Zone. The top of the succession (*D. mammilatum* zones, NC8B), is characterized successively by a sharp increase of the $\delta^{13}C_{carb}$ values, then a decrease, and finally a new increase. Both $\delta^{13}C_{carb}$ general curves and characteristic isotope shifts resemble carbon isotope segments/units previously described by Menegatti et al. (1998) and Herrle et al. (2004). This allows to propose correlations and labelling with reference to these segments/units is proposed for the EAB (Fig. 9). The labelling of the lowermost part of the $\delta^{13}C_{carb}$ curve recorded in the Ida w Shayq section, to C1 and C2, was based on the works of Stein et al. (2012, Fig. 5).

6.5. Comparison of Aptian–early Albian bio- and carbon isotope stratigraphies of the EAB with other basins

The calibration of nannofossil record to that of ammonite as well as carbon isotope stratigraphy for all studied sections in the EAB, resulted in a coherent integrated stratigraphic scheme, synthetized on a composite succession presented in Fig. 13. This scheme is compared with those of other Tethyan sections/settings where both bio- and carbon isotope stratigraphies were provided and with that of the Vocontian Basin (SE France, northern Tethys) proposed by Herrle el al. (2004), where a high-resolution carbon isotope stratigraphy was established (Fig. 13).

The absolute values of each $\delta^{13}C_{carb}$ curve vary, due to local differences in paleoenvironments. In particular, the $\delta^{13}C_{carb}$ values recorded in the EAB (this study and Luber et al. 2019; Fig. 13), are lower (on average below 1 ‰) compared to values (on average above 1 ‰) recorded in hemipelagic and pelagic carbonate sediments deposited in the Vocontian Basin, Mazagan Plateau, Zagros Mountains (Fig. 13). Lower $\delta^{13}C_{carb}$ values may be explained by the position of the studied sections: in shallower water/coastal settings, the dis-

solved inorganic carbon (DIC) would be more depleted in ^{13}C due to a higher contribution of CO_2 produced by oxidation of organic matter. However, the trends of the $\delta^{13}C_{carb}$ signal are similar, allowing the recognition and correlation of some carbon isotope units defined by Herrle et al. (2004) in the different settings (Fig. 13).

The late Barremian is defined in the EAB by ammonites; it is characterized by an increase of the $\delta^{13}C_{carb}$ values also recognized in southwestern Iran (southern margin of the Neo-Tethys). The early Aptian is characterized by a major sedimentary discontinuity (D1) in the EAB and the gap of the earliest Aptian (*D. oglanlensis* Zone); it is then represented by the *D. forbesi* to *D. furcata* ammonite zones and NC6A and B subzones. It is associated to a first $\delta^{13}C_{carb}$ minimum at the base, and a further maximum value at the early–late Aptian boundary, as also recognized in southwestern Iran and in the northern Tethys realm (isotope segments C3 to C6 of Menegatti et al. 1998, or Ap3 to Ap6 of Herrle et al. 2004). The FO of *Eprolithus floralis*, zonal marker of the base of NC7, is diachronous with respect to ammonite biostratigraphy (within *E. martini* in the EAB, and *D. deshayesi* in the Vocontian Basin).

The late Aptian, although marked by two sedimentary discontinuities (D2 and D3), is well-calibrated in the EAB, since it is defined by four ammonite zones (*E. martini*, *P. melchioris*, *A. nolani* and lower part of *H. jacobi*) and three emended nannofossil subzones (NC7A to C). This constitutes the best biostratigraphic calibration recorded for this time interval for both the southern and northern Tethyan margins. The long-term decrease in the $\delta^{13}C_{carb}$ values (Ap8 to Ap10 of Herrle et al. 2004) is well-recognized in all settings and is calibrated to the *E. martini* Zone and lower part of the emended NC7B Subzone (EAB). In southwestern Iran, however, it starts in the *D. furcata* Zone, but the ammonite record is not well-constrained (Fig. 13). The long-term increase (Ap11 to Ap15 of Herrle et al. 2004) of the $\delta^{13}C_{carb}$ values is well-recognized in all settings and is calibrated with the upper part of the *E. martini* to the lower part of the *H. jacobi* zones in both the EAB and Vocontian Basin; the top of this increase is recorded earlier (within the *A. nolani* Zone) in southwestern Iran, where, as already mentioned, the ammonite record is not-well constrained. The carbon isotope units Ap11 to Ap15 are calibrated with the NC7 Zone (NC7B and C subzones of the present study) both in the EAB and Vocontian Basin, if we follow for this latter basin, the nannofossil boundary zones recognized by Bown in Kennedy et al. (2017), and not those of Herrle et al. (2004). As matter of fact, the latter authors used the FO of subcircular *P. columnata* and not the FO of circular *P. columnata* to define the base of the NC8 Zone, thus explaining the discrepancies in nannofossil calibration between their work and the results of both Kennedy et al. (2017) and the present study.

In the EAB, the latest Aptian is well characterized in some sections by the upper part of the *H. jacobi* Zone and the new NC7D Subzone (defined in the present study). The base of the *L. tardefurcata* Zone is placed within the sedimentary discontinuity D4. The Aptian-Albian boundary (AAB) lies within the NC8A Subzone both in the EAB and the Vocontian Basin. The carbon isotope unit Al1 defined by Herrle et al. (2004), characterized by a marked decrease of the $\delta^{13}C_{carb}$ values, is well correlated in the different settings; it encompasses the AAB except in southwestern Iran, where it is supposed to be only late Aptian in age, considering the ammonite zones (Fig. 13). Calibration of the carbon isotope unit Al1 with nannofossil markers shows differences between the different sites (NC8A Subzone in the EAB; NC8A-B in the Vocontian Basin, NC8B on the Mazagan Plateau). These discrepancies may be due to different taxonomic concepts used to define the marker species *Hayesites albiensis*. As mentioned in section 6.3, only forms with long free rays should be considered as *H. albiensis* and are typical of the early Albian.

The middle part of the early Albian is well characterized in the EAB by ammonites (upper part of *L. tardefurcata* and *D. mammillatum* zones), nannofossils (NC8B Subzone) and carbon isotope record (carbon isotope units Al2–Al6 recognized). In this interval, the carbon isotope curve is in accordance with those from the Vocontian Basin, Mazagan Plateau and southwestern Iran, compared to the correlation based on biostratigraphy (Fig. 13).

7. Conclusions

A new integrated stratigraphic scheme is suggested for the latest Barremian–early Albian interval, from sections of the Essaouira-Agadir Basin (Morocco).

The distribution of ammonite assemblages of the EAB has been calibrated with the Standard Mediterranean Zonation. Index-species have been identified, in particular for the early Aptian and earliest late Aptian, which is crucial because these intervals are

dominated by condensed sedimentation and temporal hiatuses. Most of the uppermost Barremian to lower Albian ammonite zones have been recognized. The *Deshayesites oglanlensis* Zone has not been recorded, and the upper part of the upper Aptian *Hypacanthoplites jacobi* Zone and the lower part of the lower Albian *Leymeriella tardefurcata* Zone are missing.

The calcareous nannofossil record allowed to recognize four reliable new bioevents and to revise the late Aptian NC7 Zone. The NC7 Tethyan subzones have been emended and a new subzone has been introduced. Both emended and new subzones have been established through easily recognizable index species, or species occurring in various sections. The taxonomic criteria used to define the species markers of the NC8A and NC8B subzones have been specified, allowing a better calibration of these subzones with the ammonite record, with respect to previous studies.

The trends of the carbon isotope signal recorded in the six sections of the EAB are correlated. The late Aptian is characterized by highest $\delta^{13}C_{carb}$ values, whereas early Albian times are represented by minimum $\delta^{13}C_{carb}$ values; a marked decrease of the $\delta^{13}C_{carb}$ values occurs at the Aptian–Albian boundary. The recognition of some carbon isotope segments/units previously defined in the northern Tethys allowed to establish a carbon isotope stratigraphy calibrated to both ammonite and calcareous nannofossil records.

The solid biostratigraphic and chemostratigraphic scheme established for the EAB allowed rather good correlations between southern and northern Tethyan settings.

Acknowledgements. Both ammonites and nannofossil smear-slides are curated at the Collections de Géologie de l'Observatoire des Sciences de l'Univers de Grenoble (OSUG), with appropriate UJF-ID number. Most of the data presented here result from collaborative programs carried out, on one hand between the Science and Technology Development Fund (STDF) in Egypt and the Institut de Recherche pour le Développement (IRD) in France, and on the other hand between the universities of Grenoble, Agadir, Lyon and Marrakech, funded by the Ministries of foreign affairs from France and Morocco (PHC project n° 031/STU/13). These resulted in the achievement of a PhD (Hassanein 2016). We benefited from a financial support by the french IRD to W. H. K. (PhD grant) and E. J. (field trips), from annual financial supports by the ISTerre (Grenoble) and the Géologie, Terre Planètes Environnement (Lyon) laboratories, and by the OSUG@2020 Labex program of the Observatoire des Sciences de l'Univers de Grenoble. E. R. and F. G. are very grateful to J.-L. Latil and S. Reboulet for useful and friendly discussions. We are grateful to the editor Jochen Erbacher and an anonymous reviewer for both corrections and comments, which greatly improved the quality of an earlier version of the manuscript.

References

Aguado, R., Castro, J. M., Company, M., de Gea, G. A., 1999. Aptian bioevents – an integrated biostrtigraphic analysis of the Almadich Formation, Inner Prebetic Domain, SE Spain. Cretaceous Research 20, 663–683.

Aguado, R., Company, M., Sandoval, J., Tavera, J. M., 1997. Biostratigraphic events at the Barremian/Aptian boundary in the Betic Cordillera (southern Spain). Cretaceous Research 18, 309–329.

Algouti, A., Algouti, A., Taj-Eddine, K., 1999. Le Sénonien du Haut Atlas occidental, Maroc: sédimentologie, analyse séquentielle et paléogéographie. Journal of African Earth Sciences 29, 643–658.

Allan, J. R., Matthews, R. K., 1982. Isotope signatures associated with early meteoric diagenesis. Sedimentology 29, 797–817.

Ambroggi, R., 1963. Etude géologique du versant méridional du Haut Atlas occidental et de la plaine du Souss. Notes du Service géologique du Maroc 157, 1–322.

Ambroggi, R., Breistroffer, M., 1959. Stratigraphie du Crétacé du Haut Atlas occidental (Sud marocain). Cong. Geologico intern, XXè Session, Mexico, 1956, 33–40.

Beaufort, L., 1991. Adaptation of the random settling method for quantitative studies of calcareous nannofossils. Micropalaeontology 37, 415–418.

Ben Chaabane, N., Khemiri, F., Soussi, M., Latil, J.-L., Robert, E., Belhajtaher, I., 2019. Aptian-Lower Albian Serdj carbonate platform of the Tunisian Atlas: Development, demise and petroleum implication. Marine and Petroleum Geology 101, 566–591.

Ben Fahdel, M., Layeb, M., Hedfi, A., Ben Youssef, M., 2011. Albian oceanic anoxic events in northern Tunisia: Biostratigraphic and geochemical insights. Cretaceous Research 32, 685–699.

Ben Fadhel, M., Zouaghi, T., Amri, A., Ben Youssef, M., 2014. Radiolarian and planktic foraminifera biostratigraphy of the Early Albian organic rich beds of Fahdene Formation, Northern Tunisia. Journal of Earth Science 25, 45–63.

Bergen, J. A., 1994. Berriasian to eraly Aptian calcareous nannofossils from the Vocontian trough (SE Franceà and deep sea drilling site 534: new nannofossil taxa and a summary of low-latitude biostratigraphic events. Journal of Nannoplankton Research 16, 59–69.

Bergen, J. A., 1998. Calcareous nannofossils from the lower Aptian historical stratotype at Cassis-La-Bédoule (SE, France). Géologie Méditerranéenne 25, 227–255.

Bouatmani, R., Chakor Alimi, A., Medina, F., 2007. Subsidence, évolution thermique et maturation des hydrocarbures dans le bassin d'Essaouira (Maroc) : apport de la

modélisation. Bulletin de l'Institut Scientifique de Rabat 29, 15–36.

Bown, P. R., 2005. Early to mid-Cretaceous calcareous nannoplankton from the northwest Pacific Ocean, ODP Leg 198, Shatsky Rise. In: Bralower, T. J., Premoli Silva, I., Malone, M. J. (Eds.), Proceedings of Ocean Drilling Project, Scientific Results, Ocean Drilling Program, Collège Station, TX, 1–82.

Bown, P. R., Rutledge, D. C., Crux, J. A., Gallagher, L. T., 1998. Lower Cretaceous. In: Bown, P. R. (Ed.), Calcareous nannofossil biostratigraphy. British Micropalaeontological Society Publications Series, Chapman and Hall/ Kluwer Academic Publishers, 86–102.

Bralower, T. J., 1987. Valanginian to Aptian calcareous nannofossil stratigraphy and correlation with the upper M-sequence magnetic anomalies. Marine Micropaleontology 11, 293–310.

Bralower, T. J., 1988. Calcareous nannofossil biostratigraphy and assemblages of the Cenomanian-Turonian boundary interval: implications for the origin and timing of oceanic anoxia. Palaeoceanography 3, 275–316.

Bralower, T. J., Leckie, R. M., Sliter, W. V., Thierstein, H. R., 1995. An integrated Cretaceous microfossil biostratigraphy. Society of Economic Paleontologists and Mineralogists, Special Publications 50, 65–79.

Bralower, T. J., Sliter, W. V., Arthur, M. A., Leckie, R. M., Allard, D. J., Schlanger, S. O., 1993. Dysoxic/anoxic episodes in the Aptian-Albian (Early Cretaceous). The Mesozoic Pacific: geology, tectonics, and volcanism. American Geophysical Union Monograph 77, 5–37.

Bréhéret, J. G., Caron, M., Delamette, M., 1986. Niveaux riches en matière organique dans l'Albien vocontien; quelques caractères du paléoenvironnement, essai d'interprétation génétique. Documents du Bureau de Recherche Géologique et Minière 110, 141–191.

Brives, A., 1905. Contribution à l'étude géologique de l'Atlas marocain. Bulletin de la Société géologique de France 5, 379–398.

Bulot, L. G., Latil, J.-L., Hairabian, A., Fournillon, A., 2014. New insight on the genus *Nolaniceras* Casey, 1961 (Ammonoidea, Cretaceous) and its consequences on the biostratigraphy of the Aptian Stage. Proceedings of the Geologists'Association 125, 227–232.

Butt, A., 1982. Micropaleontological bathymetry of cretaceous of western Morocco. Palaeogeography, Palaeoclimatology, Palaeoecology 37, 235–275.

Canérot, J., Cugny, P., Peybernès, B., Rahli, I., Rey, J., Thieuloy, J.-P., 1986. Comparative study of the Lower and Mid-Cretaceous sequences on different maghrebian shelves and basins: Their place in the evolution of the North African, Atlantic and Neotethysian margins. Palaeogeography, Palaeoclimatology, Palaeoecology 55, 213–232.

Casey, R., 1965a. A monograph of the Ammonoïdea of the Lower Greensand. Part IV. Palaeontogical Society, 217–288.

Casey, R., 1965b. A monograph of the Ammonoïdea of the Lower Greensand. Part VI. Palaeontogical Society, 399–546.

Casey, R., 1998. Observations on the lithostratigraphy and ammonite succession of the Aptian (Lower Cretaceous) Lower Greensand of Chale Bay, Isle of Wight, UK. Cretaceous Research 19, 511–535.

Daoudi, L., Ouajhain, B., Rocha, F., Rhouta, B., Chafiki, D., 2010. Comparative influence of burial depth on the clay mineral assemblage of the Agadir-Essaouira basin (Western High Atlas, Morocco). Clay Minerals 45, 413–427.

Davison, I., 2005. Central Atlantic margin basins of North West Africa: Geology and hydrocarbon potential (Morocco to Guinea). Journal of African Earth Sciences 43, 254–274.

Kaenel, E., Bergen, J. A., 1996. Mesozoic calcareous nannofossil biostratigraphy from Sites 897, 899, and 901, Iberia Abyssal Plain: new biostratigraphic evidence. In: Whitmarsh, R. B., Sawyer, D. S., Klaus, A., Masson, D. G. (Eds.), Proceedings of the Ocean Drilling Project, Scientific Results, 149, Ocean Drilling Program, Collège Station, TX, 27–59.

Delamette, M., Caron, M., Bréhéret, J. G., 1986. Essai d'interpretation genetique des facies euxiniques de l'Eo-Albien de Bassin Vocontien (SE France) sur la base de donnees macro- et microfauniques. Comptes Rendus de l'Académie des Sciences Paris 302, 1085–1090.

Delanoy, G., 1997. Biostratigraphie des faunes d'Ammonites à la limite Barrémien-Aptien dans la région d'Angles-Barrême-Castellane. Etude particulière de la famille des Heteroceratina Spath, 1922 (Ancylocertina, Ammonoidea). Annales du Muséum d'Histoire naturelle de Nice tome XII, 270 p.

Deres, F., Achéritéguy, J., 1980. Biostratigraphie des Nannoconidés. Bulletin du Centre de Recherches et d'Exploration Production Elf Aquitaine 4, 1–53.

Dubourdieu, G., 1956. Etude géologique de la région de l'Ouenza (Confins Algéro-Tunisiens). Publications du Service de la Carte Géologique d'Algérie 10, 659 p.

Douvillé, H., 1916. Les terrains secondaires dans le massif du Moghara à l'est de l'isthme de Suez : Paléontologie. Mémoires de l'Académie des Sciences de l'Institut de France série 2, 54, 1–184.

Dutour, Y., 2005. Biostratigraphie, évolution et renouvellements des ammonites de l'Aptien supérieur (Gargasien) du bassin vocontien (Sud-Est de la France). Ph. D. Thesis, Université Claude Bernard Lyon 1, France, 302 p. (unpublished)

El Araby, A., 1999. Facies analysis and sequence stratigraphy of the Late Aptian-Albian Risan Aneiza Formation in northern Sinai. Egyptian Journal of Geology 34, 151–181.

Elkhazri, A., Abdallah, H., Razgallah, S., Moullade, M., Kuhnt, W., 2013. Carbon-isotope and microfaunal stratigraphy bounding the Lower Aptian Oceanic Anoxic Event 1a in northeastern Tunisia. Cretaceous Research 39, 133–148.

Elkhazri, A., Razgallah, S., Abdallah, H., Ben Haj Ali, N., 2009. L'événement anoxique "OAE 1a" Barrémo-Aptien en Tunisie nord-orientale : Intérêt des foraminifères. Revue de Paléobiologie 28, 93–130.

Erba, E., 1988. Aptian-Albian calcareous nannofossil biostratigraphy of the Scisti a Fucoidi cored at Piobbico (central Italy). Rivista Italiana Paleontologia Stratigraphica 94, 249–284.

Erba, E., Channell, J. E. T., Claps, M., Jones, C., Larson, R. L., Opdyke, B., Premoli Silva, I., Riva, A., Salvini, G., Torricelli, S., 1999. Integrated stratigraphy of the Cismon Apticore (Southern Alps, Italy): a reference section for the Barremian-Aptian interval at low latitudes. Journal of Foraminiferal Research 29, 371–391.

Essafraoui, B., Ferry, S., Groshény, D., Içame, N., Al Aouli, H., Masrour, M., Bulot, L. G., Géraud, Y., Aoutem, M., 2015. Sequence stratigraphic architecture of marine to fluvial deposits across a passive margin (Cenomanian, Atlantic margin, Morocco, Agadir transect). Carnets de Géologie 15, 137–172.

Ettachfini, El M., 1992. Le Vraconien, Cénomanien et Tuyronien du Bassin d'Essaouira (Haut Atlas occidental, Maroc). Ph. D. Thesis, Université Paul Sabatier, Toulouse, France, 245 p.

Ettachfini, E. M., Souhlel, A., Andreu, B., Caron, M., 2005. La limite Cénomanien-Turonien dans le Haut Atlas central. Maroc. Geobios 38, 57–68.

Fernando, A. G. S., Okada, H., 2007. New calcareous nannofossil species from the Cretaceous Budden Canyon Formation, Great Valley Sequence, northern California (USA). Journal of Nannoplankton Research 29, 1–4.

Ferreira, J., Mattioli, E., Suchéras-Marx, B., Giraud, F., Duarte, L. V., Pittet, B., Suan, G., Hassler, A., Spangenberg, J. E., 2019. Western Tethys Early and Middle Jurassic calcareous nannofossil biostratigraphy. Earth Science Review 197, 102908.

Ferry, S., Masrour, M., Grosheny, D., 2007. Le Crétacé de la marge atlantique marocaine (région d'Agadir). Excursion of the Groupe Français du Crétacé, field guidebook, 70 pp., https://hal.archives-ouvertes.fr/hal-00686791/fr/

Flügel, E., 2004. Diagenesis, porosity, and dolomitization. In: Flügel, E. (Ed.), Microfacies of carbonate rocks, Springer, Berlin, Heidelberg, 267–338.

Frizon de Lamotte, D., Saint Bezar, B., Bracène, R., 2000. The two main steps of the Atlas building and geodynamics of the western Mediterranean. Tectonics 19, 740–761.

Frizon de Lamotte, D., Zizi, M., Missenard, Y., Hafid, M., El Azzouzi, M., Maury, R. C., Charrière, A., Taki, Z., Benammi, M., Micard, A., 2008. The Atlas System. In: Michard, M. et al. (Eds.), Continental Evolution: The Geology of Morocco. Lecture Notes in Earth Sciences 116, 133–202.

Geisen, M., Bollmann, J., Herrle, J. O., Mutterlose, J., Young, J. R., 1999. Calibration of the random settling technique for calculation of absolute abundances of calcareous nannoplankton. Micropalaeontology 45, 437–442.

Gentil, L., 1905. Observations géologiques dans le sud marocain. Bull. Soc. Géol. Fr. 5, 521–523.

Giraud, F., Pittet, B., Grosheny, D., Baudin, F., Lecuyer, C., Sakamoto, T., 2018. The palaeoceanographic crisis of the Early Aptian (OAE 1a) in the Vocontian Basin (SE France). Palaeogeography, Palaeoclimatology, Palaeoecology 511, 483–505.

Godet, A., Hfaiedh, R., Arnaud-Vanneau, A., Zghal, I., Arnaud, H., Ouali, J., 2014. Aptian palaeoclimates and identification of an OAE1a equivalent in shallow marine environments of the southern Tethyan margin: Evidence from Southern Tunisia (Bir Oum Ali section, Northern Chott Chain). Cretaceous Research 48, 110–119.

Gouiza, M., 2011. Mesozoic source-to-sink systems in NW Africa: Geology of vettical movements during the birth and growth of the Morrocan rifted margin. Ph.D Thesis, Wömann: Vrije Universiteit, the Nerherlands, 150 p.

Guiraud, R., Bosworth, W., Thierry, J., Delplanque, A., 2005. Phanerozoic geological evolution of Northern and Central Africa: an overview. Journal of African Earth Sciences 43, 83–143.

Hafid, M., Aït Salem, A., Bally, A. W., 2000. The western termination of the Jebilet-High Atlas system (offshore Essaouira Basin, Morocco). Marine and Petroleum Geology 17, 431–443.

Hafid, M., Tari, G., Bouhadioui, D., El Moussaid, I., Aït Salem, A., Nahim, M., Dakki, M., 2008. Atlantic Basins-Michard, A. et al., Continental Evolution: the Geology of Morocco. Lecture Notes in Earth Sciences 116, 303–329.

Haq, B. U., 2014. Cretaceous eustasy revisited. Global and Planetary Change 113, 44–58.

Hardenbol, J., Thierry, J., Farley, M. B., Jacquin, T., de Graciansky, P.-C., Vail, P. R., 1998. Mesozoic and Cenozoic sequence chronostratigraphic framework of European Basins. SEPM Special Publication 60, 3–13, and Appendix 763–781.

Hassanein, W., 2016. The Aptian-Albian transgression in the Agadir-Essaouira Basin, Xestern Morocco. PhD Thesis, Université Grenoble Alpes, Grenoble, France, 308 p.

Heldt, M., Bachmann, M., Lehmann, J., 2008. Microfacies, biostratigraphy, and geochemistry of the hemipelagic Barremian-Aptian: influence of the OAE 1a on the southern Tethys margin. Palaeogeography, Palaeoclimatology, Palaeoecology 261, 246–260.

Herrle, J. O., 2002. Mid-Cretaceous paleoceanographic and paleoclimatologic implications on black shale formation of the Vocontian Basin and Atlantic. Evidence from calcareous nannofossils and stable isotopes. Tübinger Mikropaläontologische Mitteilungen 27, 114.

Herrle, J. O., Kössler, P., Friedrich, O., Erlenkeuser, H., Hemleben, C., 2004. High-resolution carbon isotope records of the Aptian to Lower Albian from SE France and the Mazagan Plateau (DSDP Site 545): a stratigraphic tool for paleoceanographic and paleobiologic reconstruction. Earth and Planetary Science Letters 218, 149–161.

Herrle, J. O., Mutterlose, J., 2003. Calcareous nannofossils from the Aptian-early Albian of SE France: Paleoecological and biostratigraphic implications. Cretaceous Research 24, 1–22.

Jaillard, E., Al Yacoubi, L., Reboulet, S., Robert, E., Masrour, M., Bouchaou, L., Giraud, F., El Hariri, K., 2019b. Late Barremian eustacy and tectonism in the

western High Atlas (Essaouira-Agadir Basin), Morocco. Cretaceous Research 93, 225–244.

Jaillard, E., Bouillin, J.-P., Ouali, J., Dumont, T., Latil, J.-L., Chihaoui, A., Zghal, I., 2013. The "Albian Crisis" in Central Tunisia: Nature and chronology of the deformations. Journal of African Earth Sciences 85, 75–86.

Jaillard, E., Bouillin, J.-P., Ouali, J., Dumont, T., Latil, J.-L., Chihaoui, A., 2017. Albian deformation in Central Tunisia: Evidences for an Atlantic-type passive margin. Journal of African Earth Sciences 135, 220–234.

Jaillard, E., Hassanein Kassab, W., Giraud, F., Robert, E., Masrour, M., El Hariri, K., Aly, M. F., 2019a. Aptian – lower Albian sedimentation in the Essouira-Agadir basin, western Morocco. Cretaceous Research 102, 59–80.

Jati, M., Grosheny, D., Ferry, S., Masrour, M., Aoutem, M., Içame, N., Gauthier-Lafaye, F., Desmares, D., 2010. The Cenomanian-Turonian boundary event on the Moroccan Atlantic margin (Agadir basin): Stable isotope and sequence stratigraphy. Palaeogeography, Palaeoclimatology, Palaeoecology 296, 151–164.

Jenkyns, H. C., 1996. Relative sea-level change and carbon isotopes: data from the Upper Jurassic (Oxfordian) of central and southern Europe. Terra Nova 8, 75–85.

Jenkyns, H. C., Clayton, C. J., 1986. Black shales and carbon isotopes from the Tethyan Lower Jurassic. Sedimentology 33, 87–106.

Kennedy, W. J., 2004. On *Brancoceras* Steinmann 1881 (Brancoceratidae) and *Pseudobrancoceras* gen. nov., (type species *Ammonites versicostatus* Michelin, 1838: Lyelliceratinae) from the Albian (Cretaceous) of the western Paris Basin and Provence, France. Acta Geologica Polonica 54, 251–271.

Kennedy, W. J., Gale, A. S., Bown, P. R., Caron, M., Davey, R. J., Gröcke, D., Wray, D. S., 2000. Integrated stratigraphy across the Aptian-Albian boundary in the Marnes bleues, at Col de Pré-Guittard, Arnayon (Drôme), and at Tartonne (Alpes-de-Haute-Provence), France: a candidate Global Boundary Stratotype Section and Boundary Point for the base of the Albian Stage. Cretaceous Research 21, 591–720.

Kennedy, W. J., Gale, A. S., Huber, B. T., Petrizzo, M. R., Bown, P. R., Barchetta, A., Jenkyns, H. C., 2014. Integrated stratigraphy across the Aptian/Albianboundary at Col de Pré-Guittard (southeast France). A candidate global boundary stratotype section. Cretaceous Research 51, 248–259.

Kennedy, W. J., Gale, A. S., Huber, B. T., Petrizzo, M. R., Bown, P. R., Jenkyns, H. C., 2017. The Global Boundary Stratotype Section and Point GSSP) for the base of the Albian Stage, of the Cretaceous, the Col de Pré-Guittard section, Arnayon, Drôme, France. Episodes 40, 177–188.

Kilian, W., Gentil, L., 1906. Découverte de deux horizons crétacés remarquables au Maroc. Comptes Rendus sommaires de l'Académie des Sciences de Paris 142, 603–605.

Kilian, W., Gentil, L., 1907. Sur l'Aptien, le Gault et le Cénomanien et sur les caractères généraux du Crétacé inférieur et moyen de l'Atlas occidental marocain. Comptes rendus sommaires de l'Académie des Sciences de Paris 144, 49–51.

Latil, J.-L., 2011. Lower Albian ammonites from Central Tunisia and adjacent areas of Algeria. Revue de Paléobiologie 30, 321–429.

Lemoine, P., 1905. Missions dans le Maroc occidental. Publications du Comité du Maroc, Paris, 224 p.

Le Roy, P., Guillocheau, F., Piqué, A., Morabet, A. M., 1998. Subsidence of the Atlantic Moroccan margin during the Mesozoic. Canadian Journal of Earth Sciences 35, 476–493.

Le Roy, P., Piqué, A., 2001. Triassic-Liassic Western Morocco synrift basins in relation to Central Atlantic opening. Marine Geology 172, 359–381.

Luber, T. L., Bulot, L. G., Redfern, J., Frau, C., Arantegui, A., Masrour, M., 2017. A revised ammonoid biostratigraphy for the Aptian of NW Africa: Essaouira-Agadir Basin. Cretaceous Research 79, 12–34.

Luber, T. L., Bulot, L. G., Redfern, J., Nahim, M., Jeremiah, J., Simmons, M., Bodin, S., Frau, C., Bidgood, M., Masrour, M., 2019. A revised chronostratigraphic framework for the Aptian of the Essaouira-Agadir Basin, a candidate type section for the NW African Atlantic Margin. Cretaceous Research 93, 292–317.

Luciani, V., Cobianchi, M., Lupi, C., 2006. Regional record of a global oceanic anoxic event OAE1a on the Apulian Platform margin Gargano Promontory, southern Italy. Cretaceous Research 27, 754–772.

Marshall, J. D., 1992. Climatic and oceanographic isotopic signals from the carbonate rock record and their preservation. Geological Magazine 129, 143–160.

Masrour, M., Aoutem, M., Atrops, F., 2004. Succession des peuplements d'échinides du Crétacé inférieur dans le Haut Atlas atlantique (Maroc) ; révision systématique et intérêt stratigraphique. Geobios 37, 595–617.

Medina, F., 1994. Evolution structural du Haut-Atlas Occidental et des regions voisines du Trias à l'actuel. Dans le cadre de l'ouverture de l'Atlantique central et la collision Afrique-Europe. Unpublished Doctorate. Doctorat de 3ème Cycle, Univ. Mohammed V, Rabat, Morocco, 271 p.

Medina, F., 1995. Syn- and post-rift evolution of the El Jadida-Agadir Basin (Morocco): Constraints for the rifting models of the Central Atlantic. Canadian Journal of Science 32, 1273–1291.

Mehdi, K., Griboulard, R., Bobier, C., 2004. Rôle de l'halocinèse dans l'évolution du bassin d'Essaouira (Sud-Ouest marocain). Comptes Rendus Géoscience 336, 587–595.

Menegatti, A. P., Weissert, H., Brown, R. S., Tyson, R. V., Farrimond, P., Strasser, A., Caron, M., 1998. High-resolution $\delta^{13}C$ stratigraphy through the early Aptian "Livello Selli" of the Alpine Tethys. Paleoceanography 13, 530–545.

Moreno Bedmar, J. A., Company, M., Bover-Arnal, T., Salas, R., Delanoy, G., Martinez, R., Grauges, A., 2009. Biostratigraphic characterization by means of ammonoids of the lower Aptian Oceanic Anoxic Event

(OAE 1a) in the eastern Iberian Chain (Maestrat Basin, eastern Spain). Cretaceous Research 30, 864–872.

Moreno Bedmar, J. A., Company, M., Bover-Arnal, T., Salas, R., Delanoy, G., Maurasse, J.-F., Grauges, A., Martinez, R., 2010. Lower Aptian ammonite biostratigraphy in the Paestrat Basin (Eastern Iberian Chain, Eastern Spain). A Tethyan transgressive record enhanced by synrift subsidence. Geologica Acta 8, 281–299.

Moret, L., Mahmoud, I. G., 1953. Nouvelles observations stratigraphiques et paléontologiques sur l'Albien du massif du Moghara (Sinaï-Egypte). Travaux du Laboratoire de Géologie de Grenoble 31, 269–274.

Moss, S. J., Tucker, M. E., 1996. Dolomitization associated with transgressive surfaces – a mid-Cretaceous example. Sedimentary Geology 107, 11–20.

Moullade, M., Tronchetti, G., Granier, B., Bornemann, A., Kuhnt, W., Lorenzen, J., 2015. High-resolution integrated stratigraphy of the OAE 1a and enclosing strata from core drillings in the Bedoulian stratotype (Roquefort-La-Bédoule, SE France). Cretaceous Research 56, 119–140.

Murphy, M. A., 1967. The Aptian-Cenomanian members of the ammonite genus *Tetragonites*. University of California publications in Geological Sciences 69, 1–93.

Mutterlose, J., 1991. Das Verteilungs- und Migrationsmuster des kalkigen Nannoplanktons in der Unterkreide (Valangin – Apt), NW Deutschlands. Paläeontographica Abhandlungen B 221, 27–152.

Mutterlose, J., Bornemann, A., Luppold, F. W., Owen, H. G., Ruffell, A., Weiss, W., Wray, D., 2003. The Vöhrum section (northwest Germany) and the Aptian/Albian boundary. Cretaceous Research 24, 203–252.

Perch-Nielsen, K., 1985. Mesozoic calcareous nannofossils. In: Bolli, H. M., Saunders, J. B., Perch-Nielsen, K. (Eds.), Plankton Stratigraphy, Cambridge University Press, Cambridge, 329–426.

Pervinquière, L., 1907. Étude de paléontologie tunisienne. 1: Céphalopodes des terrains secondaires. Mémoires de la carte géologique de Tunisie, 438 p.

Peybernes, C., Giraud, F., Jaillard, E., Robert, E., Masrour, M., Aoutem, M., Içame, N., 2013. Calcareous nannofossil productivity and carbonate production on the southern tethyan margin (Morocco) during the Late Aptian-Early Albian: paleoclimatic implications. Cretaceous Research 39, 149–169.

Piqué, A., Le Roy, P., Amrhar, M., 1998. Transtensive synsedimentary tectonics associated with ocean opening: the Essaouira-Agadir segment of the Moroccan Atlantic margin. Journal of the Geological Society, London 155, 913–928.

Reboulet, S., Szives, O., Aguirre-Urreta, B., Barragan, R., Company, M., Frau, C., Kakabadze, M. V., Klein, J., Moreno-Bedmar, J. A., Lukeneder, A., Pictet, A., Plock, I., Raisossadat, S. N., Vasicek, Z., Baraboshkin, E. J., Mitta, V. V., 2018. Report on the 6th International Meeting of the IUGS Lower Cretaceous Ammonite Working Group, the Kilian Group (Vienna, Austria, 20th August 2017). Cretaceous Research 91, 100–110.

Révész, K. M., Landwehr, J. M., 2001. $\delta^{13}C$ and $\delta^{18}O$ isotopic composition of $CaCO_3$ measured by continuous flow isotope ratio mass spectrometry: statistical evaluation and verification to Devils Hole core DH-11 calcite. Rapid Communications in Mass Spectrometry 16, 2102–2114.

Rey, J., Canérot, J., Rocher, A., Taj-Eddine, K., Thieuloy, J.-P., 1986. Le Crétacé inférieur sur le versant nord du Haut-Atlas (région d'Imi n'Tanout et Amizmiz) données biostratigraphiques et évolutions sédimentaires. Revue de la Faculté des Sciences de Marrakech 183, 393–441, spec. PICG-UNESCO n° 183.

Rey, J., Canérot, J., Peybernès, B., Taj-Eddine, K., Thieuloy, J.-P., 1988. Lithostratigraphy, biostratigraphy and sedimentary dynamics of the Lower Cretaceous deposits on the northern side of the western High Atlas (Morocco). Cretaceous Research 9, 141–158.

Robert, E., Peybernès, B., Bulot, L. G., 2001. Caractérisation d'une nouvelle sous-zone d'ammonite au passage Aptien-Albien dans les "Marnes noires à *Hypacanthoplites*" des Pyrénées espagnoles. Géobios 34 (1), 53–62.

Roch, E., 1930. Histoire stratigraphique du Maroc. Notes et Mémoires du Service géologique du Maroc 80, 440 p. p.

Ropolo, P., Moullade, M., Gonnet, R., Conte, G., Tronchetti, G., 2006. The Deshayesitidae Stoyanov, 1949 (Ammonoidea) of the Aptian stratotype region at Cassis-la-Bédoule (SE France). Carnets de Géologie, CG2006_M01, doi: 10.4267/2042/4744

Roth, P. H., 1978. Cretaceous nannoplankton biostratigraphy and oceanography of the northwestern Atlantic Ocean. In: Benson, W. E., Sheridan, R. E. et al. (Eds.), Initial Reports of the Deep Sea Drilling Project 44, 731–760.

Roth, P. H., 1983. Jurassic and Lower Cretaceous calcareous nannofossils in the western North Atlantic (Site 534): biostratigraphy, preservation, and some observations on biogeography and paleoceanography. In: Sheridan, R. E., Gradstein, F. M. et al. (Eds.), Initial Reports of the Deep Sea Drilling Project 76, U. S. Government Printing Office, Washington, 587–621.

Stein, M., Westermann, S., Adatte, T., Matera, V., Fleitmann, D., Spangenberg, J. E., Föllmi, K. B., 2012. Late Barremian–Early Aptian palaeoenvironmental change: The Cassis-La Bédoule section, southeast France. Cretaceous Research 37, 209–222.

Stets, J., Wurster, P., 1982. Atlas and Atlantic – Structural Relations. In: von Rad, U., Hinz, K., Sarnthein, M., Seibold, E. (Eds.), Geology of the Northwest African Continental Margin, Springer, Berlin, Heidelberg, 69–85.

Szives, O., Fodor, L., Fogarasi, A., Köver, Sz., 2018. Integrated calcreous nannofossil and ammonite data from the upper Barremian-lower Albian of the northeastern Transdanubian Range (central Hungary): Stratigraphical implications and consequences for tectonic events. Cretaceous Research 91, 229–250.

Tari, G., Jabour, H., 2013. Salt tectonics along the Atlantic margin of Morocco. Geological Society, London, Special Publication 369, 337–353.

Thierstein, H. R., 1973. Lower Cretaceous calcareous nannoplankton biostratigraphy. Abhandlungen der Geologischen Bundesanstalt 29, 1–52.

Thomsen, E., 1987. Lower Cretaceous calcareous nannofossil biostratigraphy in the Danish Central Trough. Danmarks Geologiske Undersegelse Series A 20, 1–89.

Vincent, B., van Buchem, F. S. P., Bulot, L. G., Immenhauser, A., Caron, M., Baghbani, D., Huc, A. Y., 2010. Carbon-isotope stratigraphy, buiostratigraphy and organic matter distribution in the Aptian-Lower Albian successions of southwest Iran (Dariyan and Kazhdumi formations). GeoArabia Special Publications 4, 139–197.

Wiedmann, J., Butt, A., Einsele, G., 1978. Cretaceous stratigraphy, environment, and subsidence history at the Moroccan continental margin. In: von Rad, U., Hinz, K., Seibold, E. (Eds.), Geology of the Northwest African continental margin, 3626–395, Springer, Berlin.

Wiedmann, J., Butt, A., Einsele, G., 1982. Cretaceous stratigraphy, environment, and subsidence history at the Moroccan continental margin. In: von Rad, U. et al. (Eds.), Geology of the Northwest African Continental Margin. Springer-Verlag, 366–395.

Wiegand, G. E., 1984. Calcareous nannofossils from the north-west African margin, Deep Sea Drilling Project Leg 79. In: Hinz, K., Winterer, E. L. et al. (Eds.), Initial Reports of the Deep Sea Drilling Program 79, 563–578.

Witam, O., 1998. Le Barrémien-Aptien de l'Atlas Occidental (Maroc): lithostratigraphie, biostratigraphie, sédimentologie, stratigraphie séquentielle, géodynamique et paléontologie. Strata 30, 1–421, Toulouse.

Young, J. R., Lees, J. A., 2017. Nannotax3 website. International Nannoplankton Association., Accessed 21 Apr. 2017. URL: http://www.mikrotax.org/Nannotax3.

Zühlke, R., Bouaouda, M.-S., Ouajhain, B., Bechstädt, T., Leinfelder, R., 2004. Quantitative Meso/Cenozoic development of the eastern Central Atlantic continental Shelf, western High Atlas, Morocco. Marine and Petroleum Geology 21, 225–276.

Manuscript received: February 03, 2020
Revisions required: April 21, 2020
Revised version received: May 15, 2020
Manuscript accepted: May 18, 2020

The pdf version of this paper includes an electronic supplement

Please save the electronic supplement contained in this pdf-file by clicking the blue frame above. After saving rename the file extension to .zip (for security reasons Adobe does not allow to embed .exe, .zip, .rar etc. files).

Table of contents – Electronic Supplementary Material (ESM)

Dataset. It contains data of the 233 samples recovered from the six studied sections of the Essaouira-Agadir Bain (Morocco). Each name of the 6 sheets provided in this table corresponds to the name of one section. The data set includes the age, both ammonite and calcareous nannofossil zones/subzones, carbon and oxygen isotopes, semi-quantitative/quantitative nannofossil total abundance, nannofossil preservation and semi-quantitative abundance/percentage of each identified species. Preservation of nannofossils was evaluated following the codes described by Roth (1983), allowing a categorization as follow: E3, heavily etched; E2, moderately etched; E1, slightly etched; O3, heavily overgrown; O2, moderately overgrown; O1, slightly overgrown. The semi-quantitative analysis of nannofossils was performed with a light-transmitting microscope at 1250 X magnification. Each category represents the abundance in terms of specimens per field of view (FOV), estimated over 100 FOV in a slide under using a logarithmic-like scale, following that used by Erba and Quadrio (1987). These different categories are: **Total abundance**. A: abundant (>20 specimens per FOV); C: common (10-20 specimens per FOV); F: frequent (5-10 specimens per FOV); R: rare (2-5 specimens per FOV); B: barren (no specimen found). **Species abundance**. A: abundant (more than 1 specimen per FOV); C: common (1 specimen in 1–10 FOV); F: frequent (1 specimen in 11–30 FOV); R: rare (1 specimen in 31–100 FOV); VR: very rare (less than 1 specimen in 100 FOV); B: barren (not observed in the FOV).